LASER & PHOTONICS REVIEWS
www.lpr-journal.org

All-dielectric Metasurfaces and Their Applications in the Terahertz Range

*Danni Hao, Jinwei Liu, Pinggen Zou, Yi Zhang, Ramiro Moro, and Lei Ma**

In the rapidly evolving terahertz (THz) technology field, all-dielectric metasurfaces (ADMs) have emerged as a significant driving force, potentially can transform various industries and scientific disciplines. This review offers a comprehensive and in-depth examination of the underlying principles, materials, fabrication techniques, and state-of-the-art design methods associated with THz ADMs, including the emerging role of artificial intelligence in their development. The diverse applications are delved into of these metasurfaces, such as high-resolution imaging, advanced sensing, and the development of tunable devices, showcasing the versatility and promise of ADMs in the THz range. Furthermore, the significance of interdisciplinary collaboration is discussed and the integration of cutting-edge technologies in pushing the boundaries of ADM-based THz devices. As the field continues to grow and innovate, the applications and implications of all-dielectric metasurfaces in the terahertz range are expected to become increasingly diverse, paving the way for transformative breakthroughs across various sectors.

1. Introduction

In the last decades, the terahertz (THz) spectrum (0.1–10 THz) located between the microwave and infrared regions has attracted particular interest due to its unique properties such as large available bandwidth, nonionizing photon energy, large penetration depth through materials, and capability of fingerprinting molecules' vibration modes.[1] These features make them highly desirable for applications in communication networks,[2,3] biochemical sensing,[4] material analysis,[5,6] and high-resolution imaging.[7,8] However, in the THz range, only a few natural materials have reasonably intense wave-matter interaction and functional response.[9,10] Therefore, THz devices with engineered parodic sub-wavelength structures, called metamaterials (MMs), have been intensively developed to manipulate and modulate THz radiation.

In electromagnetics, MMs are engineered to obtain the intended properties from artificial structures rather than directly from their constituent materials.[11] They have been promising candidates to produce functional components in the terahertz regime.[12–17] In the year 2000, the first double-negative ($\epsilon < 0, \mu < 0$) metamaterials operating at 5 GHz was experimentally realized through a double split-ring resonator with an array of continuous metallic wires.[18] Its negative refraction index could, in principle, could create superlens and other promising imaging applications beyond the diffraction limit.[19] Metasurfaces, as variations of MMs, usually consist of two-dimensional arranged subwavelength structures. Compared to 3D or multilayer MMs, they are less bulky and easier to fabricate using lithography with one-step direct laser writing techniques.[20–22]

Conventional metasurfaces are made with metallic structures to exploit surface plasmons, i.e., the collective oscillations of free electrons, to produce strong light-matter interactions, achieving manipulation of light.[23] By designing metasurfaces with plasmonic building blocks, many exotic electromagnetic properties have been realized. However, the cost of such an approach is an inevitable increase in light absorption, resulting in heating that has impeded many practical device applications.[24] In contrast, dielectric metasurfaces are based on resonances of the displacement current. And, at the boundary between materials with low and high refractive index, internal reflection takes place; hence, electromagnetic energy is stored as standing waves. Therefore, compared to their metallic counterparts, all-dielectric metasurfaces (ADMs) are free of Ohmic losses and have much higher efficiency.[25,26] Meanwhile, their fabrication process can be simple and compatible with the modern semiconductor industry. As a result, ADMs are promising in overcoming some vital physical and engineering issues.

This paper presents a concise progress review of ADMs that work in the THz frequency range from physical principles and an overview of the materials and fabrication approaches for applications that have emerged in recent years. Section 2 begins with the background of the light-matter interaction for metasurface's building blocks (meta-atoms) and metasurfaces. Section 3 introduces the materials and fabrication procedures used in ADM devices. Section 4 briefly introduces advanced design methods

D. Hao, J. Liu, P. Zou, Y. Zhang, R. Moro, L. Ma
Tianjin International Center for Nanoparticles and Nanosystems
Tianjin University
Tianjin 300072, China
E-mail: lei.ma@tju.edu.cn
L. Ma
Tianjin Key Laboratory of Low-dimensional Electronic Materials and Advanced Instrumentation
Tianjin, China

The ORCID identification number(s) for the author(s) of this article can be found under https://doi.org/10.1002/lpor.202301210

DOI: 10.1002/lpor.202301210

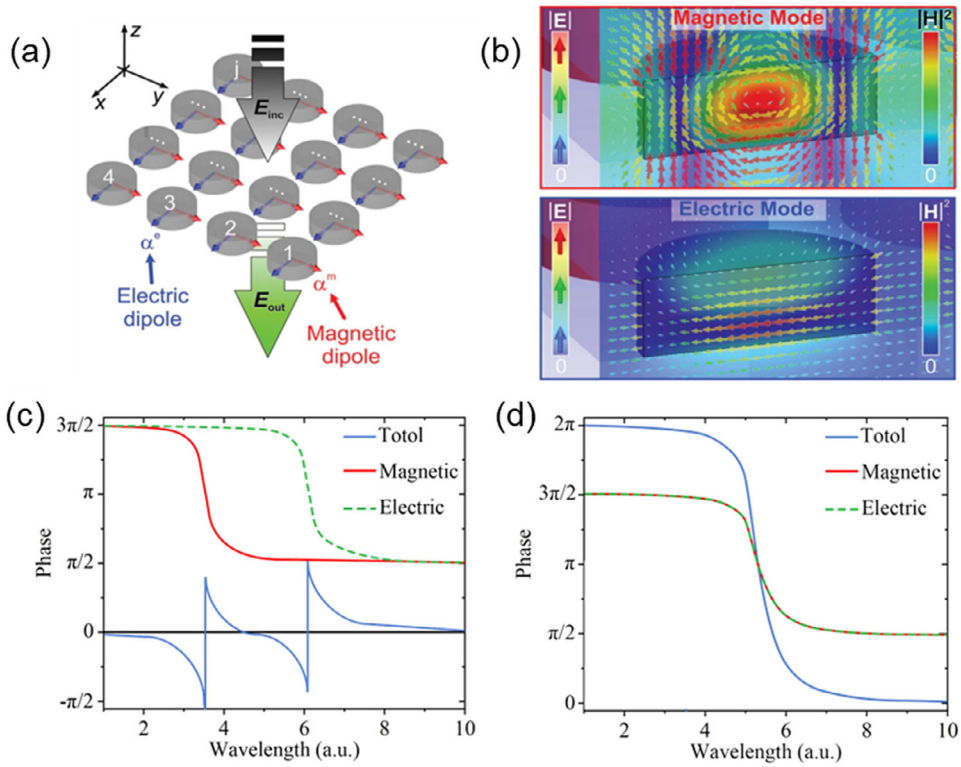

Figure 1. a) Array of dielectric disk resonators illuminated by a linear polarized electromagnetic wave (electric field is x-polarized) at normal incidence. The dielectric resonators are represented as electric and magnetic dipoles with the polarizabilities $\boldsymbol{a^e}$ and $\boldsymbol{a^m}$. b) Electric and magnetic field distribution of a single silicon disk. The electric field is represented by colored arrows and the magnetic field is represented by color. The top and bottom figures correspond to the magnetic and electric modes dominated by magnetic and electric dipole moments. c) and d) show the phase spectra of the total transmitted field (blue), the electric (green dash), and magnetic (red) response within two scenarios. In (c), the magnetic and electric modes are separated. And for (d), the magnetic and electric modes overlap and achieve a continuous $2\boldsymbol{\pi}$ phase shift due to the constructed interference of the electric and magnetic dipole resonances. Reproduced with permission.[30] Copyright 2015, WILEY-VCH Verlag GmbH & CO. KgaA.

such as AI assistant ADM design. Section 5 describes some major applications of all-dielectric metasurface-based devices and discusses the emergence of tunable and programmable devices. To conclude, current challenges are discussed and the future development of ADM technology is envisioned in Section 6.

2. Light-Matter Interaction in Dielectric Meta-Atoms and Metasurfaces

2.1. Mie Resonances and Wavefront Control

As mentioned in the last section, novel designs using dielectric materials can break the limits of plasmonic metasurfaces. Rather than adopting plasmonic structures typically made from noble metals such as gold and silver, low-cost dielectric materials with high refractive indices can tune the behavior of electromagnetic waves through Mie resonances.[27–29] Like plasmonic resonance, the resonant frequency also depends on the shape, materials, and optic properties of the surrounding media in the dielectric resonators.

To illustrate the principle of dielectric resonators, disk structures are taken as an example, as shown in **Figure 1a**. Unlike plasmonic resonators, the two lowest resonant modes supported by the dielectric disks are electric and magnetic dipole resonances.[30] The magnetic dipoles are generated by the circular displacement current of the electric field, which is induced by the penetrating field and phase retardation inside the dielectric structures. This happens when the wavelength of incident radiation is comparable to the structure's dimensions, $\lambda / n_s = D_s$, where λ is the wavelength, n_s is the refractive index of the material and D_s is the disk diameter. As illustrated in Figure 1b, the electric and magnetic fields are mainly distributed inside the disks. For the first Mie resonance (electric dipole), the displacement current in the disk produces a large circulating magnetic field. For the second Mie resonance (magnetic dipole), the circulating displacement current leads to a strong magnetic polarization in the center of the disk. The circular electric field surrounds the magnetic field and modulates the magnetic permeability $\mu(\omega)$ of the metasurface. At the same time, the circular magnetic field around the electric field modulates the electric permittivity $\varepsilon(\omega)$. Therefore, the electric and magnetic dipole resonances can be treated as artificial atoms, i.e., meta-atoms, which make the metasurface with arbitrary values of $\mu(\omega)$ and $\varepsilon(\omega)$.[31]

Considering the unique properties of Mie resonances, we can further explore the phase control and interference of electromagnetic waves when interacting with resonant structures. As shown in Figure 1c, taking advantage of charge oscillations of Mie resonant structures, when the frequency is below the first electric

dipole frequency (around a wavelength of $\lambda/6$ in Figure 1c), the charge follows the excitation in phase, when it is right at the resonance, it oscillates $\pi/2$ behind the driving field, and when it is over the resonance frequency, a full π phase delay is introduced.

Having discussed the phase behavior of Mie resonances, we can now examine how to achieve precise control of the wavefront by using the principles of Huygens' metasurfaces and dielectric resonators. A single resonance provides a full π phase shift. By an elaborate geometric design, it is possible to shift the electric and magnetic dipole resonant frequencies and coincide them in certain values.[30,32,33] Based on Huygens' Principle, every point on a wavefront can be treated as a new source of wavelets, the secondary waves spread out with speed equal to the propagation of the source wave, and the line tangent of the secondary waves gives the new wavefront. Combining the concept of Huygens' principle and the power of the dielectric resonator that can provide 2π phase shifts. As Figure 1d demonstrates that the overlap of the magnetic and electric modes resulted in a continuous 2π phase shift due to the constructed interference of the electric and magnetic dipole resonances. Electromagnetic waves interacting with resonant structures can gain different phase shifts and interfere with each other. Thus, the wavefront of the new wave can be controlled.[34] Meanwhile, when the electric and magnetic dipole moments are perpendicular to each other, the scattered field will be unidirectional, which meets the requirement for realizing reflection-free Huygens' metasurfaces.

2.2. Theories of Coupled Resonators

Besides dielectric metasurfaces based on dipolar resonance modes, coupled resonators that exhibit Fano resonances have also gained interest due to their sharp spectral features that give narrow linewidths and high Quality factors (Q-factors), which can benefit applications requiring high sensitivity.[35] The Fano resonance is typically the result of interference between a broad resonance mode or a continuum band with a narrow discrete resonance.[36,37] This can be achieved by breaking the symmetry of coupled resonators,[38] such as the asymmetric bowtie silicon resonators (as seen in **Figure 2b**). The opposite current densities in the upper and bottom resonators, produce a net dipole moment, which can be used as a bright mode. A quadrupolar resonance can be used as the dark mode, which is spectrally sharp due to its weak coupling to the far field and having extremely low radiative losses. Therefore, the interference between the dipolar and quadrupolar modes produces a sharp Fano resonant feature.[39]

Figure 2a shows a comparison between Fano resonance and Electromagnetic Induced Transparency (EIT), illustrating the coupling scenario and line shape of each phenomenon.[40] In Figure 2b, the Fano resonance (EIT line shape) is introduced by asymmetric resonators. The Fano resonance becomes stronger and shifts to a higher frequency when the asymmetry between the two triangular structures is changed. A quadrupolar-like resonance mode can be observed in the magnetic field distribution.[39]

This phenomenon can be described by a standard three-level model (Figure 2c), which consists of three states: a ground state with no excitation $|1\rangle$, a state with a bright dipolar mode $|2\rangle$, and a state with a dark quadrupolar mode $|3\rangle$. States $|2\rangle$, and $|3\rangle$ are coupled upon radiation and give the Fano phenomena.[24,41] An ADM utilizing Fano resonances provides featured absorption or transmission spectrum when bright and dark modes interact with each other. The steep dispersion in the transmission spectrum enables electromagnetically induced transparency together with slow-light effects. EIT is considered as a special case of Fano resonance when the frequency of the two oscillation states are match.[40,42] In Figure 2d, an ADM comprising asymmetric splitring resonators and its transmission spectra in media with varying refractive indices is presented. The high Q-factor EIT resonance provides a high sensitivity of 231 GHz/RIU (Refractive Index Unit), which favors applications requiring high detection capabilities.[35]

In recent studies, Bound States in the Continuum (BIC) has increasingly garnered attention. This theory posits that any resonant state within the continuous radiation band could be elucidated using BIC.[12,43–46] Electromagnetic wave energy is confined inside meta-structure due to the resonance, therefore almost no radiation energy loss occurs, which makes the resonant state based theory has been powerful guidance for designing high-quality factor ADMs.[47,48]

2.3. Pancharatnam-Berry Phase Principle

The Pancharatnam-Berry (PB) phase, i.e., geometric phase can also be used to obtain phase modulation of electromagnetic waves. Besides linear polarization waves, the PB phase can be applied to circularly polarized waves and transform them into propagating waves with different directions or polarizations, or to create vortex beams.[49,50] Rather than changing the resonators' geometric structures, the meta-atoms of PB-phase metasurfaces introduce phase changes by identical meta-atoms arranged in varying orientations with respect to the fast axes.[51,52] To understand the modulation of polarization waves, consider that two identical resonators are placed on the x-y plane, and the second one has a rotation angle θ with respect to the first one. When irradiated with circularly polarized waves, the polarization effect can be described by the Jones matrix:

$$\boldsymbol{T}_{\theta}(x,y) = \boldsymbol{R}(\theta(x,y))\,\boldsymbol{J}(\varphi)\,\boldsymbol{R}^{-1}(\theta(x,y)) \tag{1}$$

where $\boldsymbol{J}(\varphi)$ represents the operator of a meta-atom with retardation φ and $\boldsymbol{R}$ represents the rotation matrix. When left-handed and right-handed circular polarized waves (LCP and RCP) are incident on the resonators, the scattered waves by the meta-atoms will have the following form:[51]

$$\begin{aligned}\boldsymbol{E}_{\text{output},RCP} &= \boldsymbol{T}(x,y)\,|R\rangle \\ &= \left[\cos(\varphi/2) - i\sin(\varphi/2)\exp(-i2\theta)\right]|L\rangle\end{aligned} \tag{2}$$

$$\begin{aligned}\boldsymbol{E}_{\text{output},LCP} &= \boldsymbol{T}(x,y)\,|L\rangle \\ &= \left[\cos(\varphi/2) - i\sin(\varphi/2)\exp(i2\theta)\right]|R\rangle\end{aligned} \tag{3}$$

This indicates that the spin-flipped components of the scattered waves will differ with a phase factor of $e^{i2\theta}$. So that LCP

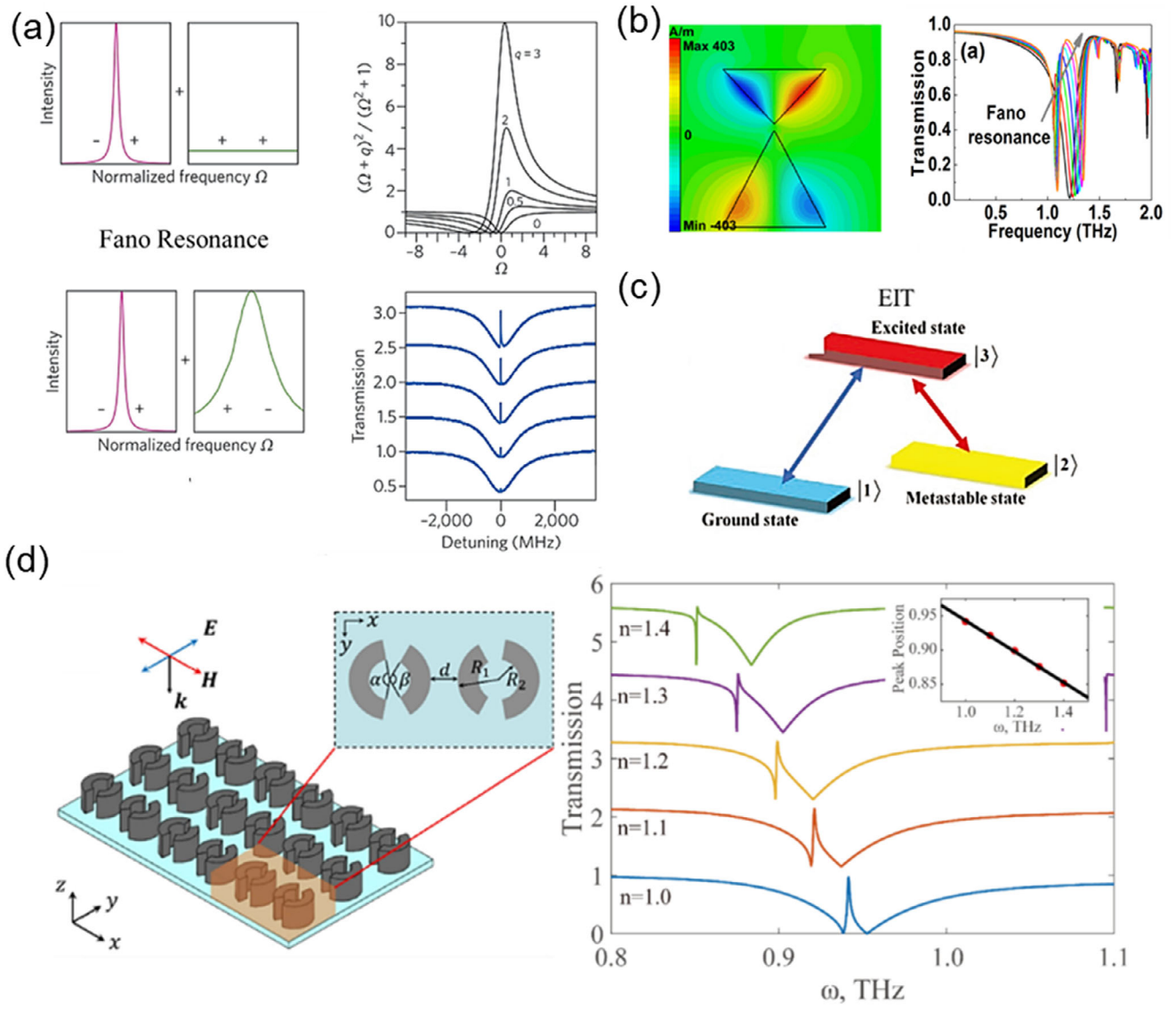

Figure 2. a) Fano resonance and EIT, coupling scenario and line-shape of each phenomenon. Reproduced with permission.[40] Copyright 2017, Springer Nature Limited. b) Fano resonance (EIT lineshape) is introduced by asymmetric resonators. The Fano resonance becomes stronger and shifts to a higher frequency when the asymmetry between the two triangular structures is changed. A quadrupolar-like resonance mode can be observed in magnetic field distribution. Reproduced with permission.[39] Copyright 2019, Optica Publishing Group. c) A three-level atomic system model used to describe the Fano resonance.[41] Copyright 2020, WILEY-VCH Verlag GmbH & Co. KGaA. d) ADM comprises asymmetric split-ring resonators and their transmission spectra in media with varying refractive indices. EIT resonance with high Q-factor gives a high sensitivity of 231 GHz/RIU.[35] Copyright 2019, Optica Publishing Group.

and RCP waves will be transformed into RCP and LCP and will gain or lose an additional phase shift of $2\theta(x, y)$.[53] By rotating the meta-atoms on the metasurface plane (x-y plane) by θ ranging from 0 to π, one can obtain a continuous phase change from 0 to 2π. PB phase modulation introduces phase shifts purely due to geometric arrangement. Thus, the shift is independent of dispersion and scattering details. Therefore, metasurfaces based on the PB-phase concept have broad bandwidth. The efficiency of the PB-phase metasurface is determined only by the meta-atom's scattering efficiency.

In the above discussion of the PB-phase metasurface, it is useful to provide visual examples for better understanding. As shown in **Figure 3**a a schematic illustration of a metasurface designed based on the PB-phase principle.[54] This metasurface consists of resonators with the same geometry but spatially varied orientations, as illustrated in (b), introducing phase shifts since the circularly polarized wave is modulated by the PB-phase.[55] Furthermore, (c) displays a scanning electron microscope (SEM) image of an ADM waveplate designed with resonators of different geometries.[56] The phase shift in this waveplate is introduced via Mie resonance independent of polarization, making it suitable for linear polarized waves. These examples illustrate the concepts discussed above and clearly represent PB-phase principle-based metasurface designs. The following section will delve into

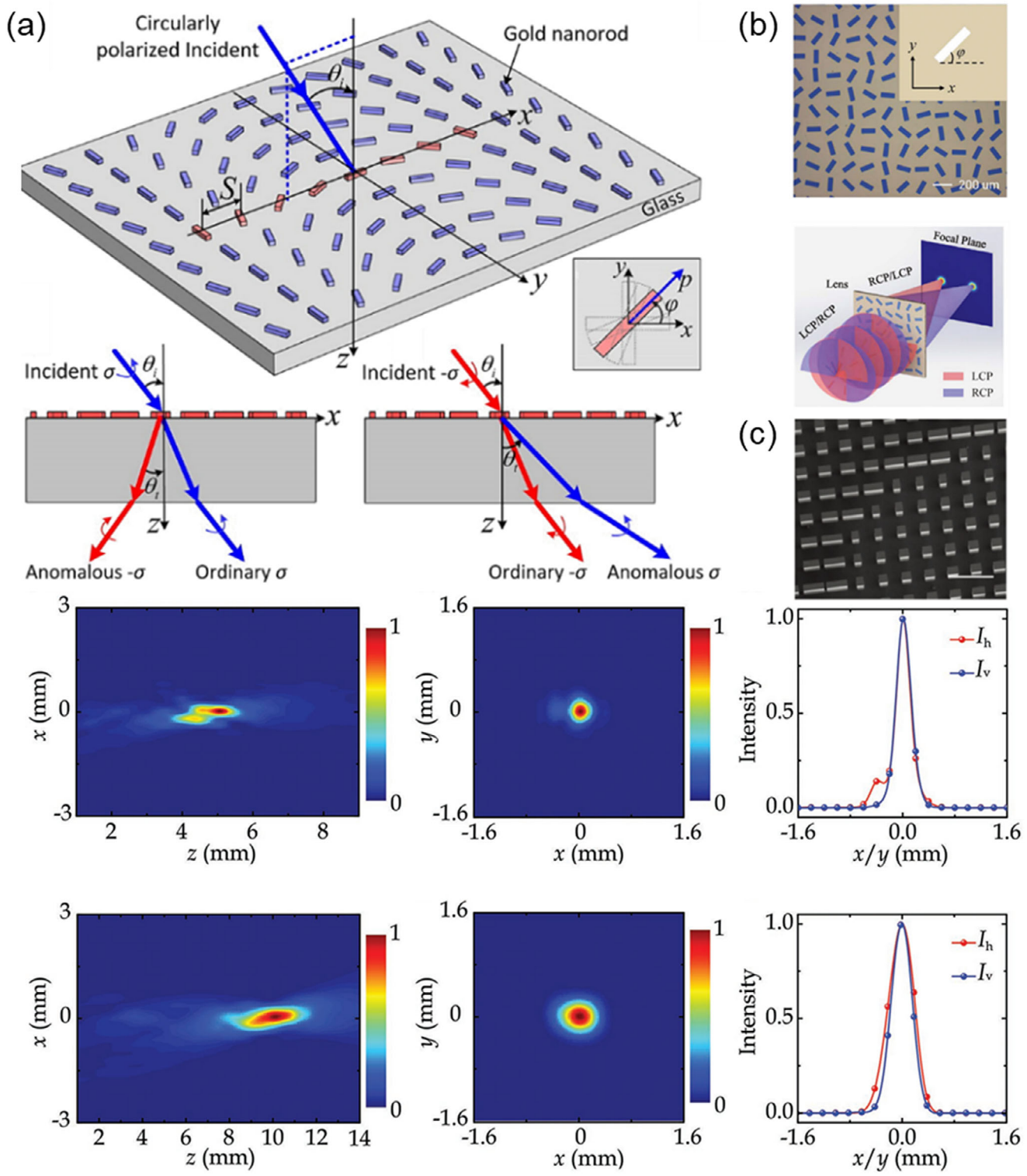

Figure 3. a) Schematic illustration of a metasurface designed based on PB-phase principle. Reproduced with permission.[54] Copyright 2012, American Chemical Society. b) Image of resonators with the same geometry placed with spatially varied orientations to introduce phase shifts. The circularly polarized wave is modulated by PB-phase. Reproduced with permission.[55] Copyright 2015, Optica Publishing Group. c) SEM image of an ADM waveplate designed with resonators of different geometries. The phase shift is introduced via Mie resonance independent of polarization. It can be used for linear polarized waves. Reproduced with permission.[56] Copyright 2017, WILEY-VCH Verlag GmbH & Co. KGaA.

Table 1. Typical all-dielectric substances in terahertz range and their properties.

Material	permittivity ϵ	Tunability	Advantages	Reference.
High-resistivity Si	≈11.7	None	mature fabrication process,low loss	[11]
Doped Si	High	None	broadens bandwidth, supports surface plasmon resonances	[57]
Strontium Titanate (STO)	High	Temperature	Low loss, Tunability	[58, 59]
Barium Titanate (BaTiO3)	≈10	Electric,Photonic,Temperature	Nonlinear response,Reliable tunability	[60, 61]
Potassium Tantalate (KTaO3)	High	Similar to STO	Similar to STO	[62–64]
Polydimethylsiloxane (PDMS)	≈1.98	Mechanical	Stretchable	[65, 66]
Polyimide	≈3.2	None	Stable performance	[57, 67, 68]
Parylene	≈3	None	Similar to Polyimide	[69]
cyclic olefin copolymer (COC)	2.34	None	Similar to Polyimide	[70]

the materials and fabrication techniques that are normally employed in ADM design to enhance their radiation efficiency.

To enhance the radiation efficiency of the metasurface, the composition of materials is an essential parameter. In the following section, we will discuss the materials and the fabrication techniques that are commonly used in ADM design.

3. Overview of Materials and Fabrication Techniques

3.1. Materials

Material selection is one of the most important factors for designing the metamaterials with desired parameters. Conventionally, metals are chosen which has the negative real component of the permittivity. As for ADM designs, high-index materials with low absorption loss are appealing; however, some materials are difficult to grow directly on certain substrates, and that limits the development of ADMs. Single-crystal Si has been widely used in ADM design thanks to its low-cost and mature fabrication process. As listed in **Table 1**, high-resistivity silicon has a high permittivity ($\epsilon \approx 11.7$) and an exceptionally low dissipation loss in the terahertz range.[11] However, it cannot be grown on metallic substrates or oxide/amorphous substrates directly, which largely limits the applications of the corresponding Si microstructures. Doped Si, as a material having rather high dissipation loss in the THz frequencies, has been exploited to improve the THz absorption efficiency and broaden the bandwidth. It shows metallicity and can support surface plasmon resonances.[57]

Strontium titanate (STO),[58,59] $BaTiO_3$,[60,61] and $KTaO_3$[63,64] are ferroelectrics that can be used as dielectric metamaterials due to their high permittivity, low dielectric losses, and large electro-optic coefficients. Besides, their relative permittivity can also be tuned through applied external electric field, magnetic field, and temperature, which makes them desirable for making tunable terahertz devices.[58,71] STO has been integrated with a silicon-based metamaterial in thin-film form for tuning the terahertz response of ADMs.[58,59]

Regarding the substrate materials, ideally, they should have low refractive indexes to minimize reflection losses and geometric aberrations of the fabricated lens. Moreover, since the strong field confinement around resonators intensely interacts with the supporting dielectric substrate, the substrate must have small losses. Although high-resistivity silicon has been commonly used in THz ADM designs with a refractive index of ≈ 3.4, it generates a power loss at the air-silicon interface of about 30% when used as substrate.[56] Moreover, it is opaque in the visible range, which is not convenient for device alignment. However, most visible range transparent materials have their own critical issues, either having strong terahertz absorption (e.g., silicate glass) or rather prominent anisotropic (e.g., sapphire and quartz). Therefore, low-loss polymers stand out as a favorite choice in terahertz applications.

PDMS can be used as the matrix for both plasmonic and dielectric composites. It is optically isotropic, transparent in the visible range, and has a weak absorption in the THz range.[65,66] It has a small thermal diffusivity, hence, could improve the spatial resolution and be used for a terahertz imaging system.[66] Its flexibility allows it to be applied in wearable devices. Similarly, such as polyimide,[57,67,68] parylene,[69] and cyclic olefin copolymer (COC)[70] also have relatively low losses across the entire terahertz spectrum, thus they can reduce insertion and dissipation losses when used as substrate and dielectric spacers.[57,67,68] The fabrication processes of polymers consist mainly of spin-coating the mixed liquid on a supporting platform and curing at ambient conditions. The thickness of the polymer can be accurately controlled by the spinning rate. Then, the film can be trimmed into the desired shape and dimensions and bonded to a supporting frame or substrate.[68]

3.2. Fabrication

Different from conventional metallic metamaterials, which are normally fabricated by deposition and lift-off processes, all-dielectric metamaterials are usually rather complicated, while, over the past few years, efforts have been devoted to fabricating ADM structures with a good balance between precision and cost.

Typically, direct laser patterning is used to achieve high-precision and mask-free patterning. Femtosecond laser micromachining techniques can also be applied to fabricate most dielectric materials. The ultrafast and high-power laser is focused on the dielectric surface and evaporates the material following the designed pattern with resolution down to sub-micrometer. Normally, the dry etching cycle combines cooling and sweeping to prevent the melting of adjacent regions and avoid residue dust. Beam aperture, pulse, and cycle numbers can be adjusted based on the desired geometry and resolution, which has been used in studying Mie resonances of silicon-based all-dielectric

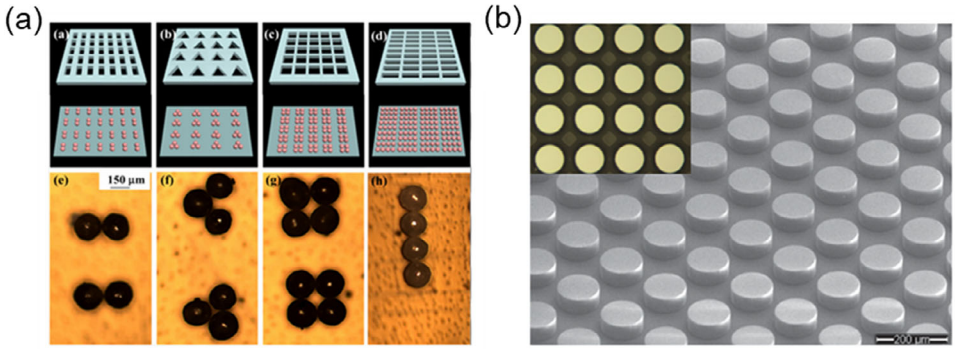

Figure 4. a) Illustration of the template-assisted self-assembly method. Dimer, trimer, tetramer, and a chain of Al_2O_3 and ZrO_2 sphere resonators are assembled on a 50 μm thick polyimide film. Reproduced with permission.[75] Copyright 2019, Optica Publishing Group. b) SEM image of Si pillars. They are etched by the Bosch DRIE technique and bonded on a PDMS film. Reproduced with permission.[82] Copyright 2017, Optica Publishing Group.

one-dimensional gratings and patterning STO single crystal plates in tunable negative permeability metamaterial devices.[72,73]

Self-assembly can also be used in ADM fabrication. The usage of this technique can be divided into two categories. One is to directly self-assemble dielectric particles with similar size to form a layer and achieve resonant electromagnetic response or to mount dielectric particles with patterned holes as template which is referred to as micro-template-assisted self-assembly as shown in **Figure 4a** [74–76] Another one is to employ microsphere lithography (MSL). The polymer spheres are self-assembled and mounted on a sample surface to serve as lithographic templates or etching masks and followed by lithography or etching to define the size and depth of the dielectric resonators. The intrinsic limitation of MSL is that the fabricated dielectric resonators can only be disks or triangles in a triangular lattice. As a result, so far, it is only used in the infrared region rather than in the THz band.[77]

The needed Resolution of lithography is normally determined by the operation wavelength of devices.[78–80] For metasurfaces working in the NIR or visible range, high-resolution techniques such as electron beam lithography (EBL), self-assembly patterning, or focused ion beam milling are required. Accordingly, for the terahertz range (3–30 mm) devices, the critical dimension is around 1 to 10 μm, which can be easily realized through low-level photolithography with large yielding and dimension production.[81] For top-down patterning of microstructures, photolithography combined with a selective etching approach is the most used method. Once the patterns are defined by exposing and developing the photoresist, selective etching can be conducted to form the desired dielectric meta-atoms. Some deep etch processes may need extra steps for hard mask preparation.

The pattern definition on the x-y plane is simple for dielectric metamaterials; however, for the z-axis, deep and anisotropic etching processes are required to achieve steep and uniform structures.[82] Bosch DRIE (deep reactive ion etching) process is often used in deep silicon etching. The cycle consists of SF_6 and C_4F_8 plasma etching, where C_4F_8 gas is used to generate a protection layer to passivate the walls, and SF_6 is for partially removing the passivation layer on the wall and all passivation layer at the bottom of the hole. Therefore, by combining and regulating the etching process, one can unidirectionally etch the Si layer and obtain vertical profiles, as shown in Figure 4b. For III–V materials, halogens chlorine, bromine, and iodine are normally used as etching gases, such as Cl_2 and BCl_3 gases being used for InSb etching of terahertz gratings.[83] Although inadequate for defining sub-micrometer features, wet etching techniques are also used in the fabrication of ADM devices. Hydrofluoric acid has been used to etch the SiO_2 buried layer and release the silicon handling layer of SOI (silicon-on-insulator).[66]

4. Advanced ADM Design Methods

In the last decade, the development of photonics, particularly metasurfaces, has revolutionized the field of optics. Numerous studies have been conducted to reveal the underlying mechanism behind light-matter interactions within subwavelength structures.[27–30,40,41] However, the complicated design procedures of metasurfaces still limit the scope and depth of their applications. One approach is to optimize the sketch design through elaborate modeling and solving Maxwell's equations, while another involves seeking a less time- and effort-consuming design process.

As shown in **Figure 5**, advanced design methods, including Machine Learning-based Design and Optimization Methods, have become crucial for the development of All-dielectric Metasurfaces (ADM) technology.[84] These methods can optimize the design process, reduce computational costs, and improve the performance of ADMs.

4.1. Machine Learning-Based Design

Machine learning-based design methods use algorithms to learn from data and make predictions or decisions. In ADM design, machine learning can be used to optimize the geometry of resonator structures based on the desired spectrum. Here, we will present some examples of machine learning techniques used in ADM design.

Deep Neural Networks (DNNs) are a class of machine learning models composed of multiple layers of interconnected artificial neurons, which allow them to learn complex patterns and relationships from the targeting data. DNNs are capable of

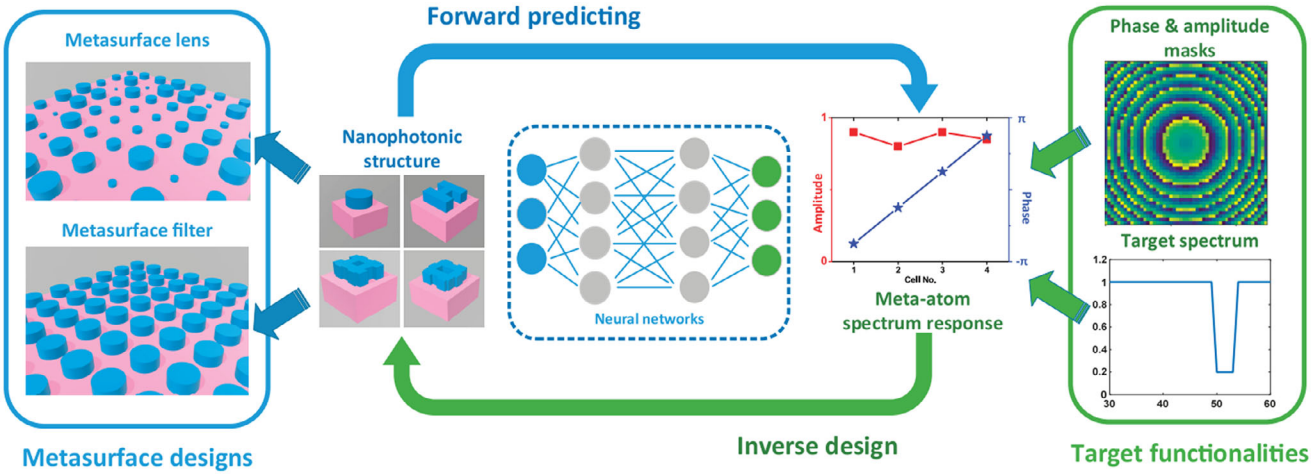

Figure 5. Advanced Design Methods for ADM: Integration of Machine Learning or Neural Networks with Optimization Algorithms, featuring precise modeling of amplitude and phase response for dielectric elements at the atomic level through forward prediction and inverse optimization for wavefront control and spectral manipulation. Reproduced with permission.[84] Copyright 2019, American Chemical Society.

modeling non-linear and high-dimensional relationships by iteratively adjusting the weights of connections between neurons through a training process that minimizes an error function. They have been used to model complex ADM systems based on both the known metasurface geometry and spectra. DNNs can also be used for inverse engineering metasurfaces, predicting the geometries of resonator structures based on the desired spectra.[84–86]

Convolutional Neural Networks (CNNs) have been found to be highly successful in computer vision applications due to their ability to process and extract hierarchical features from images. In the context of ADM design, CNNs can be employed to analyze and recognize patterns in the geometrical structures of metasurfaces. By leveraging their feature extraction capabilities, CNNs can help build accurate and efficient neural networks for predicting the desired electromagnetic properties of metasurfaces, thereby streamlining the design process.[85,87]

Recurrent Neural Networks (RNNs) are a type of neural network specifically designed to process sequential data, making them well-suited for applications that involve time series or spatially distributed data. In ADM design, RNNs have been utilized to predict the electromagnetic response of a metasurface based on its geometry. This is achieved by treating the arrangement of resonator structures as a sequence and training the RNN to learn the relationships between these structures and their resulting electromagnetic properties.[88]

Generative Adversarial Networks (GANs) are a novel type of machine learning model that can generate new data, similar to training data, by simulating the process of data generation. In the field of ADM design, GANs have been applied to create new tunable metamaterials with advanced features. By training GANs on existing metasurface designs, researchers can generate novel geometries that exhibit desired properties, such as tunable resonances or improved performance in specific applications.[89]

Machine learning-based design methods provide many advantages in the field of metasurface engineering. By leveraging their ability to learn from data and make predictions or decisions based on that data, these techniques can significantly accelerate the design process and yield more effective metasurface designs. Moreover, machine learning methods can be employed for inverse engineering of metasurfaces, allowing researchers to predict the optimal geometries of resonator structures based on the desired spectral response, which can be particularly useful in the development of tailored metasurface devices for specific applications.

4.2. Optimization Methods

Optimization methods are used to find the optimal solution to a problem by minimizing or maximizing an objective function subject to constraints. In ADM design, optimization methods can be used to find the optimal geometry of resonator structures based on the desired spectrum.

Gradient-based methods, like the gradient descent algorithm, utilize the derivative of the objective function to iteratively update the design variables until convergence to an optimal solution.[90] On the other hand, simulated annealing is a stochastic optimization method that explores the design space by incorporating randomness, which allows it to avoid being trapped in local minima and potentially find a global minimum solution.[91]

Genetic Algorithms (GAs) are a type of optimization algorithm inspired by the process of natural selection. GAs work by evolving a population of candidate solutions through iterations applying a series of operations such as selection, crossover, and mutation. In the context of ADM design, GAs can be used to optimize the geometry of resonator structures based on the desired spectra by efficiently searching the configuration space that satisfies the design objectives and constraints.[92,93]

Topology optimization is also a powerful design method that seeks to find the optimal distribution of material within a given domain, enabling the creation of high-performance metasurfaces with a broad range of capabilities. Applications of topology optimization in ADM design include high-efficiency light deflection with nearly arbitrary input and output angles, spectral sorting of plane waves to distinct diffraction orders, and light focusing with field-curvature correction.[94–97]

In addition to the techniques, other optimization methods, such as swarm intelligence and more, have also been applied to ADM design. Swarm intelligence techniques, like Particle Swarm Optimization (PSO) and Ant Colony Optimization (ACO), mimic the behavior of social organisms in nature to cooperatively search the design space and locate optimal solutions.[98–100]

4.3. Hybrid Design Approaches

Combining machine learning and optimization methods can lead to enhanced ADM design by leveraging the strengths of both approaches. For instance, machine learning can be utilized to generate initial designs or predict the performance of candidate metasurface geometries, effectively narrowing down the design space. Subsequently, optimization methods, such as numerical optimization techniques or topology optimization, can be employed to refine these initial designs and achieve superior performance.

Hybrid design approaches can provide more degrees of freedom in designing new tunable metamaterials, enabling the exploration of novel geometries and functionalities. By harnessing the power of both machine learning and optimization techniques, researchers can streamline the design process, improve efficiency, and ultimately develop more effective ADM devices.[15,84]

5. Applications

While numerous impressive achievements have been reported using advanced ADM design methods in various applications in section 4, there are still many other areas awaiting exploration. In the following sections, we will provide an overview of diverse ADM applications.

5.1. Perfect Reflector

High-efficiency reflectors act as key components in terahertz sources and detectors. For conventional metallic mirrors, around 2 % of the incident light is dissipated in the form of heat.[101] Dielectric mirrors (Bragg reflectors) are made from periodic thin layers of dielectric materials with alternating refractive indexes.[102] They can reach uniform reflection thanks to constructive interference. However, the multilayer structure requires multistage fabrication processes with a long producing period and leads to a bulky product.

B. Slovick et al. theoretically proposed a rule to achieve perfect reflection for a homogenous medium that can be applied to designing metamaterials.[103] It indicates that for a semi-infinite medium, the unity reflectance requires zero in the real part of the impedance for the medium (z_r). This requirement is satisfied when $\varepsilon_r/\mu_r < 0$ and $\varepsilon_i\ \mu_r = \varepsilon_r\ \mu_i$, where the complex permittivity and permeability are given by $\varepsilon_r + i\varepsilon_i$ and $\mu_r + i\mu_i$, respectively. For a metasurface with only electric or magnetic resonance and made of lossless materials, both conditions can be satisfied.

Accordingly, an all-dielectric metasurface based perfect near-infrared broadband reflector was developed by P. Moitra et al..[104] It consists of an array of sub-wavelength-thick Si cylinders with a hexagonal lattice on a SOI substrate. In the terahertz range, Z. Song et al. designed a single-layer dielectric reflector consisting of TiO_2 microcubes, which numerically predicts a 0.2 THz broad reflection band centered at 0.9 THz with an average reflection greater than 99%.[105] Taking advantage of electric and magnetic resonances, B Fang et al. also designed a broadband terahertz reflector, which is the very first study of the reflection performance of a single Si cylindrical resonator with different radii.[106] The single negative characteristic requirement is met in the operating frequency regime, and a wide reflection spectrum is obtained since the electric and magnetic dipole resonances are close to each other. They also used a planar arrangement to further broaden the reflection spectrum. By incorporating multiple resonators with different sizes into one unit cell, a broadband spectrum was obtained by superposing adjacent resonances. However, the coupling between neighboring resonators can lead to the appearance of a Fano resonance, which should be avoided. Later, this design strategy was also applied in other metasurface designs.[107,108]

An electric mirror will introduce a 180° phase reverse on the mirror surface; normally, this causes destructive interference and leads to an electric field minimum at reflection spots. On the contrary, a perfect magnetic conductor imposes a 2π phase change in its magnetic component and no phase change on the electric field of the reflected wave. By this means, a local maximum of the absolute electric field can be introduced at the surface ($\ll \lambda/4$) in the distance) of the perfect magnetic conductor, which leads to a stronger interaction with the electric field.[109] To take advantage of this property of a perfect magnetic conductor, D. Headland et al. designed a dielectric metasurface to enhance the device sensitivity by increasing the antenna radiation efficiency.[110]

5.2. Reflect-Array: Wavefront Engineering in Reflection Mode

Besides reinforced spectral control, metasurfaces can also manipulate the spatial profile of the incident beam. With the development of high-reflectance dielectric resonator arrays, much work has started to focus on highly efficient all-dielectric metasurfaces with beam-shaping functions operating in reflection mode.[111] Typical applications, including beam collimation, steering, and focusing, can be achieved through metasurfaces-based wavefront engineering.[112,113] The mechanism of such devices is rooted in both Huygens's principle and the generalized form of Snell's law.[114,115] A local phase shift can be imparted when a single resonator is excited by an incident wave.[116] Ideally, the phase shift range should be able to cover one 2π cycle and be immune to the interference from the adjacent resonators. Therefore, by carefully creating an arbitrary phase gradient in the reflected wavefront from the arrays of resonators, one can manipulate the profile and directionality of reflected beams.

D Headland et al. designed a metasurface composed of a dielectric resonator on a gold ground plane using SU-8 resist as the adhesive layer. This reflect-array can focus collimated radiation at 1 THz with a 3 dB bandwidth of 18 %. **Figure 6a** shows an SEM image of the reflect array (left), which can be used as a reflective beam focusing lens (right). It can also be used to collimate a terahertz beam.[117] Z Ma et al. realized a full 2π phase control

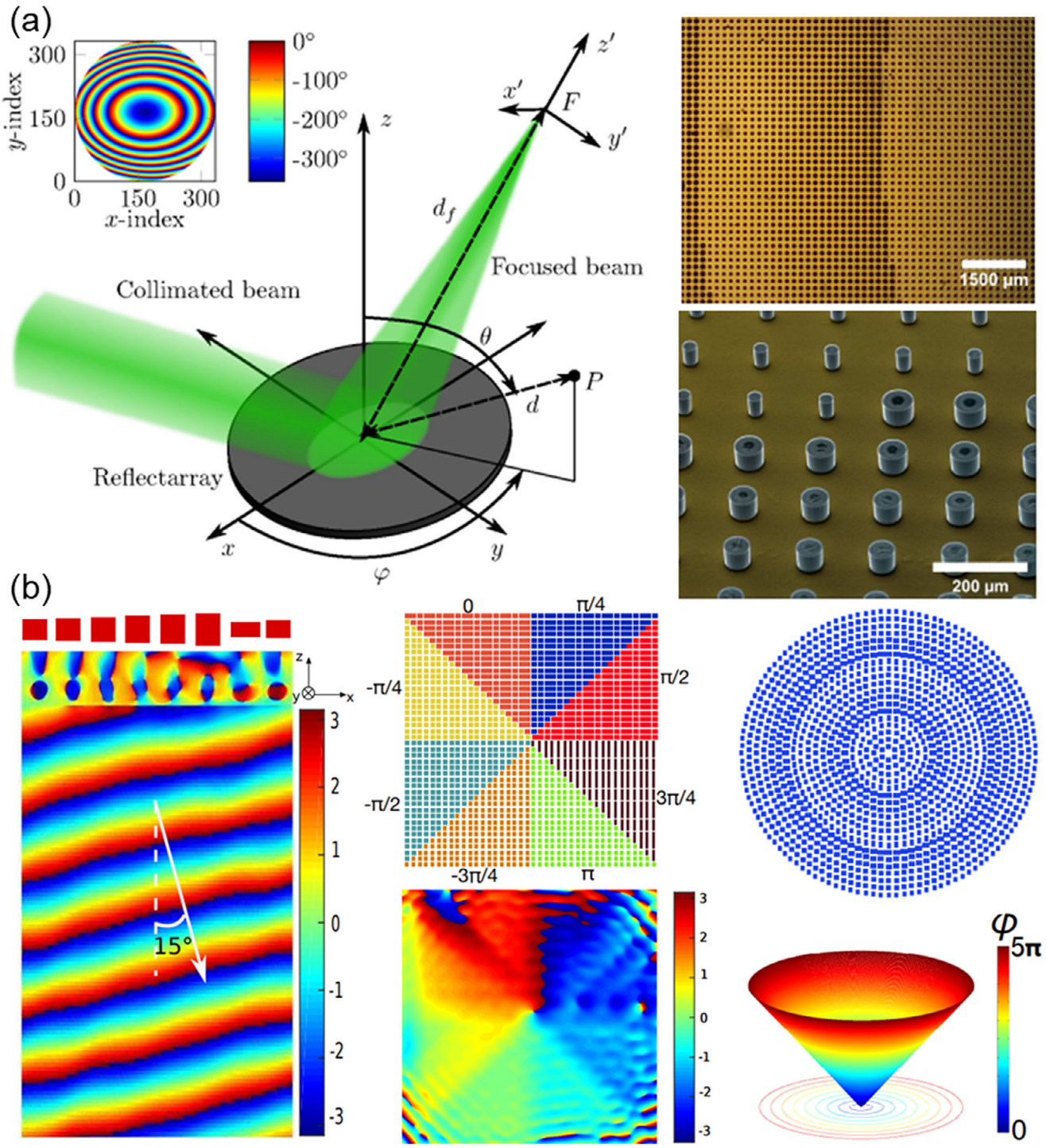

Figure 6. Reflect-array wavefront engineering in all-dielectric metasurfaces: a) SEM image of a reflect-array. The metasurface can be used as a reflective beam-focusing lens. It can also be used to collimate a terahertz beam. Reproduced with permission.[117] Copyright 2016, American Chemical Society. b) Schematic of the building blocks of the all-dielectric magnetic mirror metasurface and the layout for achieving the function of a vortex beam converter. The eight resonators can cover phase space from 0 to 2π with $\pi/4$ intervals. A metasurface with the phase variation needed to generate Bessel beams is also demonstrated. Reproduced with permission.[118] Copyright 2016, American Chemical Society.

by varying the geometries of the resonators in the transverse x and y directions, where the dielectric resonators were made of Si cubes on a silica substrate. It demonstrated that a single-layer metasurface can generate anomalous surface reflection, optical vortex beams, and Bessel beams. Figure 6b shows the schematic of the building blocks of the all-dielectric magnetic mirror metasurface and the layout for achieving the function of a vortex beam converter. The eight resonators can cover phase space from 0 to 2π with $\pi/4$ intervals. A metasurface with the phase variation needed to generate Bessel beams is also demonstrated. These results are invaluable for terahertz communications, including beam-forming and polarization control in holograms, which have large potentials in the next-generation THz communications.[118]

5.3. Transmit-Array and Metalens

Transmit arrays have gained much attention due to their ability to manipulate the shape, the directionality of incident beams, and ease of usage.[111,119] Like the reflect array, the transmit array also employs passive resonators to achieve beam control.[120] This metasurface is also referred to as metalens since its operating principle is like the phase shift induced by a conventional lens with a curved surface. Metalenses made from plasmonic micro/nanostructures experience reflection and absorption caused by Joule damping and have low transmission efficiency. On the other hand, dielectric resonators can work as phase shifters, providing a route to achieve full-range phase manipulation while circumventing the fundamental drawbacks of their metallic counterparts.[121] A radiation source consisting of both electrical and magnetic dipole moments oriented perpendicular to each other only radiates in one direction,[122] which fulfills the critical assumption in Huygens' law.[24] By simultaneous excitation of electric and magnetic dipoles, total transmission can be obtained when the overlap between electric and magnetic dipoles is achieved, realizing a perfect transmissive Huygens's surface.[30]

The phase distribution of the transmitted radiation is given by:

$$\phi(x,y) = 2m\pi + \frac{2\pi f}{\lambda} - \frac{2\pi\sqrt{f^2+x^2+y^2}}{\lambda} \quad (4)$$

where m is an arbitrary integer number, f is the focal length, and λ is the wavelength.[123] By superposition of position-dependent phase delays, the produced new wavefront can be tailored and made into artificial metalenses. D. Jia et al. equivalently discretized the continuous phase profile in the abovementioned equation into eight phase shifts and designed resonators accordingly, as shown in **Figure** 7a with a schematic diagram of the THz metalens composed of cross-shaped Si pillars.[124] The focal efficiency of the metalens is 24 %, which is higher than most plasmonic metasurface lenses. Q. Cheng et al. reported a broadband dielectric metasurface that can realize achromatic focusing in the range of 0.3 to 0.8 THz using C-shaped resonators, as illustrated in Figure 7b that displays a broadband achromatic metalens designed with C-shaped unit elements.[125] The experimental setup is also given, showing a near-field probe mounted on a motorized stage to measure the electric field distribution. In addition, this metalens exhibits a high working efficiency of more than 68 % and a numerical aperture of 0.385. The robustness of the device regarding fabrication imperfections was discussed and simulated. X. Jiang et al. demonstrated a terahertz metalens with a focal length of 300 λ, a radius of 300 λ, and a numerical aperture of 0.707, as shown in Figure 7c that presents an image of the metalens made by Si cubes on top of a Si substrate.[126] This metalen was used for imaging experiments with linearly polarized THz waves. They also demonstrated the metalens reversibility by imaging objects with forward and backward incident directions, where the letters "H" and "N" are imaged using the metalens for forward and inverse incident directions.[126]

In order to diminish the reflection losses, H. Zhang et al. designed an antireflection silicon pillar array on the backside of a metasurface, which successfully reduced the reflectance down to 0.3 %. To prove the concept, they combined two fabricated metasurface slides back to back, which shows that the measured polarization conversion efficiency increased from ≈40 % to ≈60 %.[56]

5.4. Polarization Control

Polarization control components have a critical role in THz systems. Dielectric resonators can be designed to have birefringent responses; that is, when excited by external radiation, the resonator imparts independent phase shifts to either of the orthogonal electric field components of an incident wave. Metasurfaces can then be engineered as waveplates that transform a linearly polarized incident wave into another polarization angle or from linear to circular polarization.[127–129]

J. Zi et al. proposed a metamaterial that can function as a transmissive terahertz half-wave plate. Similar to ref.[56] the design of metamaterial adopts the double-working-layer strategy to reduce the reflection from the back surface.[130] Experiments show the polarization conversion rate can reach almost 100%, and its cross-polarized transmission can reach 90% at the operation frequency of 1 THz. This can benefit various THz applications and systems.

Waveplates operating in a reflection manner instead of transmission can be referred to as birefringent mirrors. W. Lee et al. employ metasurfaces composed of subwavelength resonators to archive polarization control in a reflection manner for a 45° incidence angle.[131] Instead of conventional metallic resonators, they used low-order dielectric resonators to achieve higher radiation efficiencies, and the geometry was carefully designed to obtain a broadband response. The linear incident wave can be converted into a circularly polarized wave upon reflection, i.e., the metasurface acts as a quarter-wave mirror. A half-wave mirror made of metasurface was also demonstrated.

5.5. Vortex Beam Generator

One significant attribute of ADMs is the ease of user defining anisotropy. As shown in **Figure** 8b, The anisotropy of ADMs usually stems from engineered asymmetries of their structure. This anisotropy facilitates a high refractive index contrast between orthogonal polarized incident light which is not feasible in the natural material. It is essential for realizing polarization

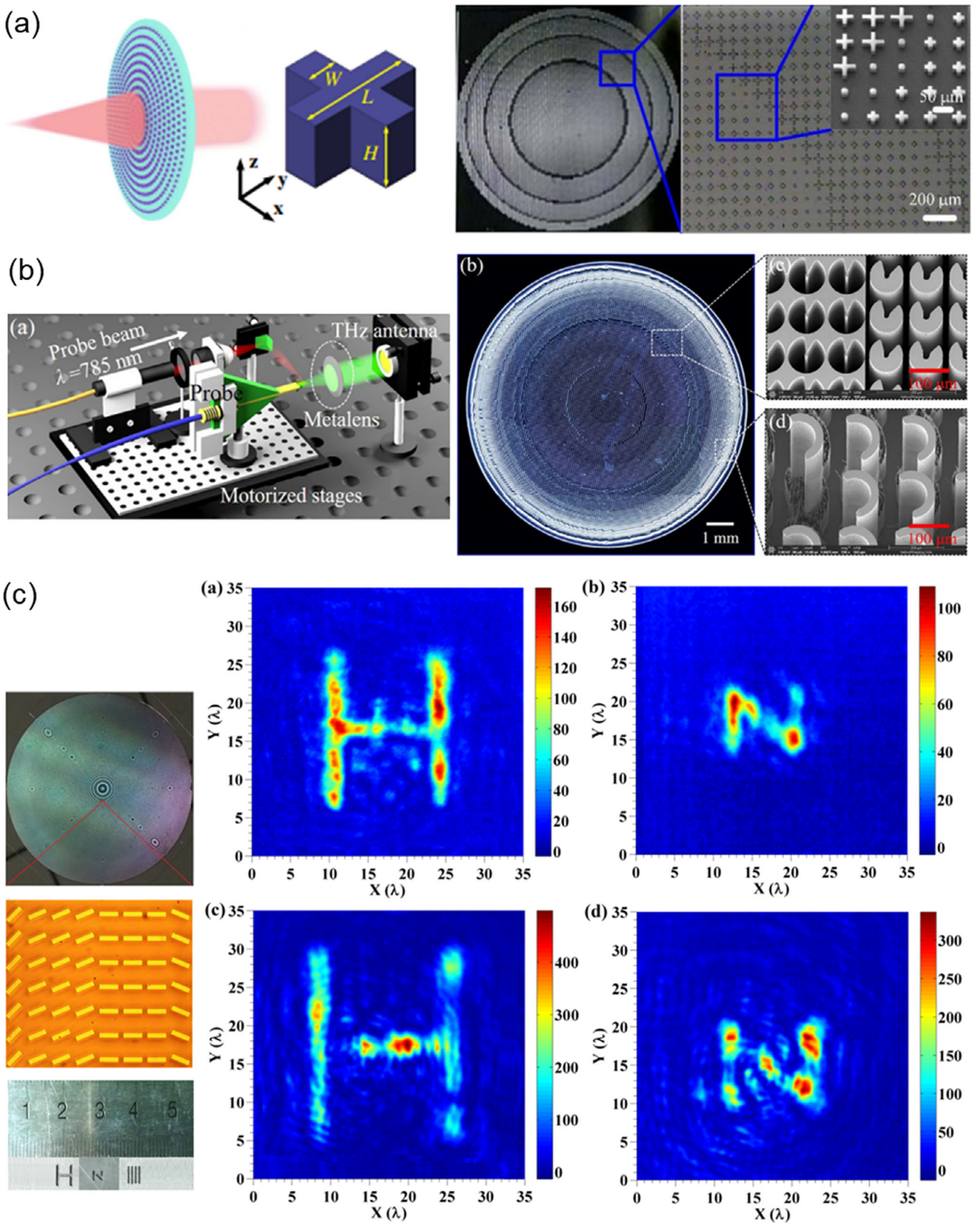

control, wavefront shaping, creating highly directional beams, and generating vortex beams in THz domain.

Orbital angular momentum (OAM) is introduced to quantum communication by increasing the degrees of freedom of a single photon, therefore, to realize the goal of expanding the information capacity carried by wireless communication signals through multiplexing. It can be performed by a spiral phase front, i.e., a vortex beam that has a cork-screw shape wavefront, and the wave's Poynting vector circulates around the beam axis following a spiral trajectory.[121] The number of OAM (l) corresponds to the number of twists of the spiral wavefront in one wavelength along the propagating direction. THz vortex beams can be employed in not only high-speed communications but also electron acceleration and high-resolution THz imaging applications.[132]

Metasurfaces are capable of controlling polarization and phase and have been successfully applied to make spin-orbit conversions. Q-plates, which are inhomogeneous waveplates, are used as geometric phase elements that transform the spin angular momentum of light into orbital angular momentum. They can transform LCP to RCP or vice versa and have $\pm 2q\hbar$ OAM, where q is the topological charge of the q-plate, $\hbar$ is the Planck's constant divided by 2π. With advanced design, metasurfaces can also be used to produce single or superposition of two total angular momentum (TAM) states and provide conversion from an arbitrary input SAM state to two arbitrary output TAM states [133] and such a device is referred as a J-plate.

Following the PB phase concept (Section 2), to build a vortex phase plate with the topological charge q, the required orientation angle distribution of meta-atoms in polar coordinates (r, α) can be calculated by $\alpha(r, \varphi) = q\varphi$. Here, α is the orientation angle of meta-atoms with respect to the x-axis in the x-y plane, and $\varphi = \arctan(y/x)$ is the azimuthal angle.[134]

Y. Xu et al. demonstrated a transmissive dielectric metasurface that can efficiently generate cylindrical vector beams using a spin-decoupled phase control method, as shown in Figure 8a with a schematic of vector vortex beam generation and vortex Bessel beam generation metasurfaces' phase distribution. The ADM design is based on spatial-variant rectangular-shaped Si pillars on Si substrates. In their proposed design, the dynamic phase is controlled by the physical dimensions of the resonator structures, and the geometric phase has also been introduced by the rotation operation applied on the resonator structures with respect to the x-y basis (PB-phase). By exploiting this arrangement, the phase responses of two circularly polarized components can be decoupled, and the superposition of two circularly polarized components inside the output beam can be controlled. By simultaneously manipulating the geometric phase and the dynamic phase, two ADMs were designed to generate vector vortex and vector Bessel beams. The average transmission efficiency of the proposed generators is less than 60 %, which is mainly attributed to the silicon substrate and can be improved by substituting the substrate with lower refractive index materials such as polymer films.[135]

Subsequently, C. Zheng et al. presented a design of ADMs made from cross-shaped Si pillar arrays on Si substrates, as illustrated in Figure 8b with an image of the chiral coding metasurface composed of cross-shaped Si pillars.[136] The metasurface could be used to realize chiral coding by combining two-phase arrangement schemes of two circularly polarized components into one design so that one circularly polarized component is scattered, and the other is transmitted and transformed into a vortex beam.

5.6. Absorber

Metamaterial absorbers can absorb electromagnetic radiation in a specific or broad band of spectrum. They are promising for designing detectors, sensors, and imaging systems in the THz band. High absorption can be achieved when the metamaterial's electric and magnetic responses are designed to match free space impedance at certain frequencies to attain nearly uniform absorption.[66] Conventional metallic metamaterial absorbers are normally composed of a metal ground plane and a patterned metal layer separated by a layer of dielectric spacer,[137] where the metal ground plane is used to suppress transmission. The metal patterns can generate electric resonance from plasmonic resonance effects, and a magnetic resonance is produced by the antiparallel current from the two metallic layers. As mentioned earlier, both electric and magnetic resonances can exist in dielectric resonators within a single dielectric layer in contrast to two metal layers with spacing required by metallic metamaterials.[138] By tuning the geometry of the dielectric metasurface, the electric and magnetic resonances can overlap, thus yielding perfect absorption.

X Liu et al. have demonstrated a high-efficiency terahertz absorber composed of Si cylindrical resonators on PDMS substrate.[82] By tailoring the geometric structures, the lowest-order electric dipole and magnetic dipole modes were tuned to overlap in frequency. So that the incident wave was absorbed entirely within the dielectric resonator layer rather than transmitted or reflected, that design realized a peak absorption efficiency of 97.5% around 1.011 THz. Like their metallic counterparts, tuning the dimension of the structure can shift the resonance into different frequencies and offer spectrally selective absorption peaks. The accumulated heat from the metamaterial absorber can also be used for imaging applications with infrared sensors. Adopting the above design, K. Fan et al. realized uncooled terahertz imaging.[66]

Dielectric absorbers have been demonstrated in other geometric forms, such as sawtooth, cubes, and annular cavities.[139,140] To broaden the absorption spectrum, doped silicon has been widely used in these devices. W.Withayachumnankul et al. designed

Figure 7. a) Schematic diagram of the THz metalens composed of cross-shaped Si pillars. Reproduced with permission.[124] Copyright 2018, Optica Publishing Group. b) Broadband achromatic metalens are designed with C-shaped unit elements. The experimental setup is also given. A near field probe is mounted on a motorized stage to measure the electric field distribution Reproduced with permission.[125] Copyright 2019, Science China Press. c) Image of the metalens made by Si cubes on top of a Si substrate. This metalen is used for imaging experiments with linearly polarized THz waves, the letters "H" and "N" are imaged using the metalens for forward- and inverse-incident directions. Reproduced with permission.[126] Copyright 2018, Optica Publishing Group.

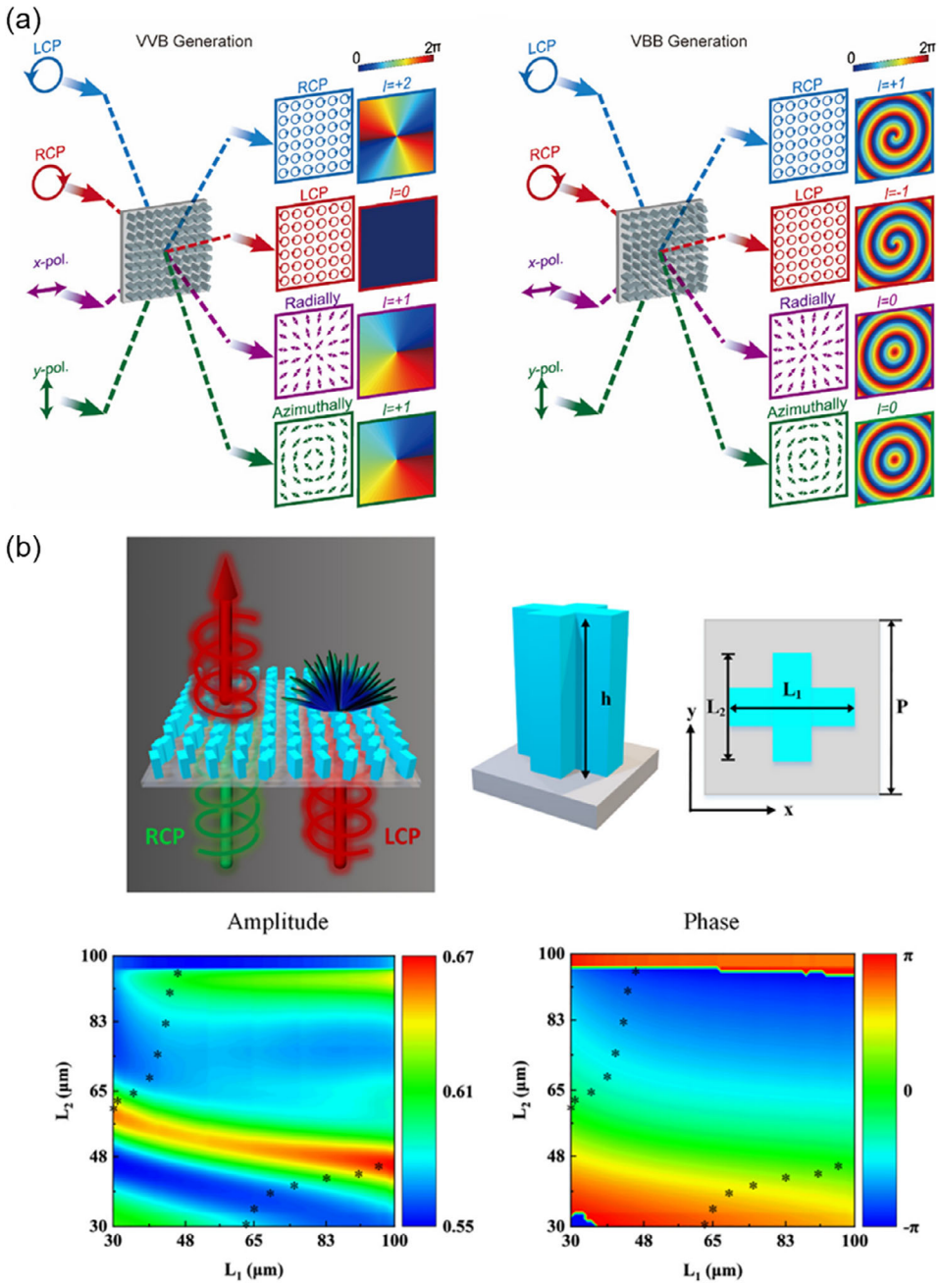

Figure 8. a) Schematic of vector vortex beam generation and vortex Bessel beam generation metasurfaces' phase distribution. Reproduced with permission.[135] Copyright 2020, Walter de Gruyter Gmb. b) Illustration of the chiral coding metasurface composed of cross-shaped Si pillars. The LCP wave is scattered after going through the metasurface, while the RCP wave is transmitted and transformed into a vortex beam. Reproduced with permission.[136] Copyright 2021, Walter de Gruyter GmbH.

a broadband absorber using the first-order coaxial surface plasmon polaritons generated by doped silicon and fundamental standing waves inside cavities. As evidenced in **Figure 9a**, the SEM images show Si cavity resonators, which have been engineered for perfect absorption. In the same figure, we compare the reflection and absorbance spectra for the metasurface with that of bare doped silicon.[91] The design of these absorbers was steered by critical coupling conditions, which is a pivotal concept in our work. In this scenario, the rate at which radiation loss declines must mirror the damping rate of the dissipation losses (expressed mathematically as $(Q_{leak}^{-1} = Q_{diss}^{-1}$). This balance ensures that all the energy from the incident wave is effectively dissipated within the structures, leading to perfect absorption.[91] Some other techniques have also been demonstrated to broaden the absorption peak, such as merging two absorption peaks from two diffraction modes.[11,140] H. Liu et al. proposed a broadband terahertz absorber composed of silicon cross resonators with internal air cavities arranged in a rectangular 2D array as

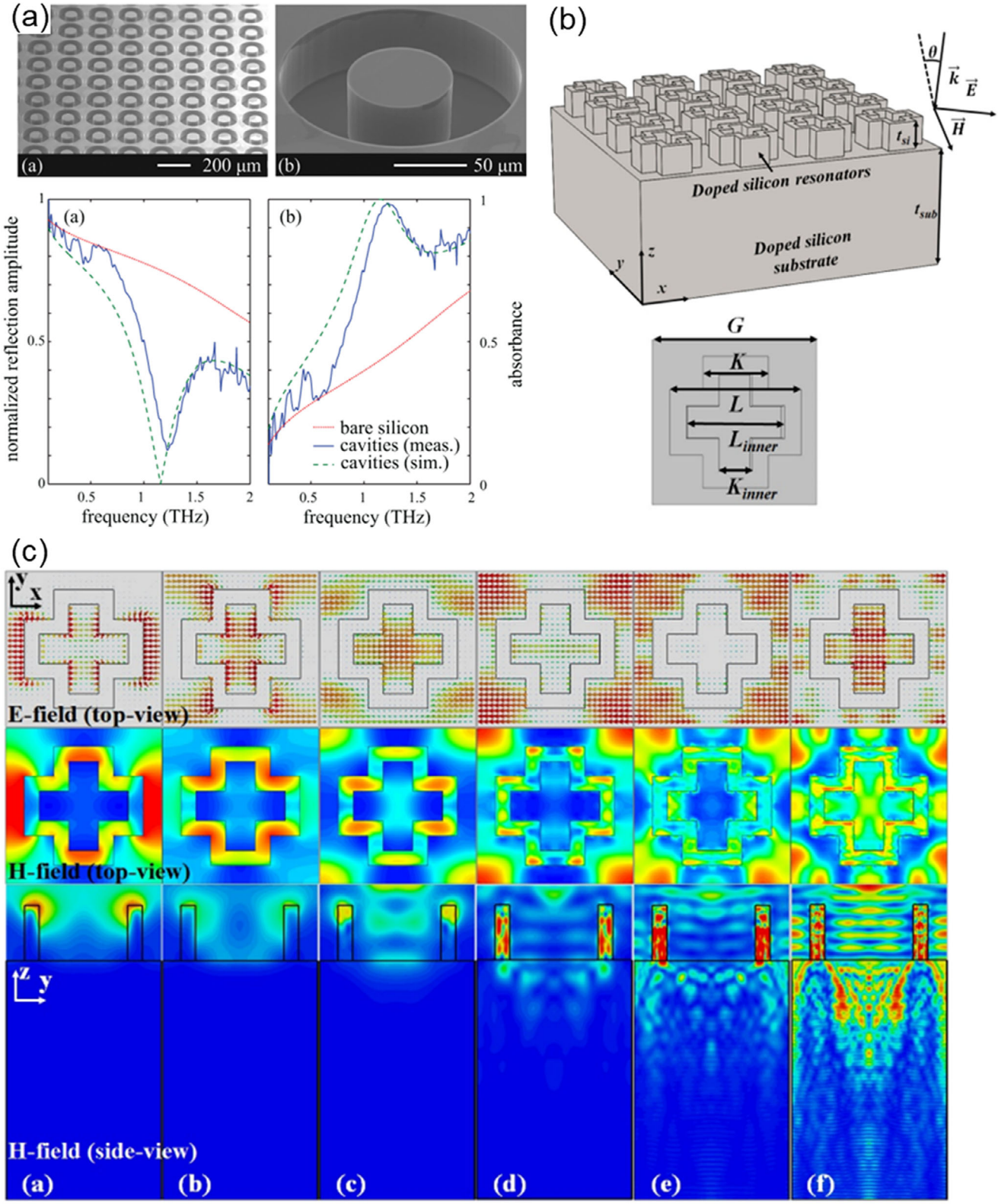

Figure 9. a) SEM images of the Si cavity resonators for perfect absorption. Reflection and absorbance spectra for the metasurface and the bare doped silicon are plotted for comparison. Reproduced with permission.[143] Copyright 2014, American Chemical Society. b) Schematic drawing of THz absorber. Reproduced with permission.[141] Copyright 2018, MDPI. c) Electric and magnetic field distribution for the absorber at different resonant frequencies. Multiple air-cavity resonant modes are responsible for the ultra-wide absorption band. Reproduced with permission.[141] Copyright 2018, MDPI.

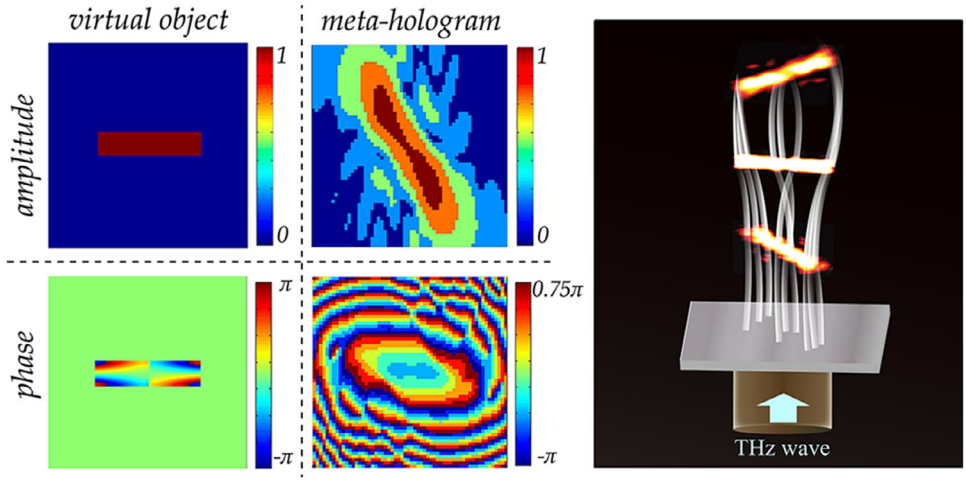

Figure 10. Meta-holography allows tailoring of both the phase and amplitude of the virtual object. The hologram can be stretched and rotated along the propagating direction of the THz wave. Reproduced with permission.[148] Copyright 2018, American Chemical Society.

illustrated in Figure 9b, which can generate plasmonic modes at four corners of the cross structure and the cavities between each cross, with electric and magnetic field distribution for the absorber at different resonant frequencies and multiple air-cavity resonant modes responsible for the ultra-wide absorption band as shown in Figure 9c. By combining these air-cavity modes and the intrinsic absorption in the substrate, a wide absorption band ranging from 0.6 to 10 THz was achieved with an average absorption of ≈95 %. Meanwhile, due to the four-fold symmetry of the metasurface, it exhibits polarization insensitivity at normal and oblique incidence.[141] S. M. Hanham et al. demonstrated that InSb touching disks also have useful plasmonic responses in the THz regime. The single dipole mode/charge transfer plasmon mode has been studied and proved to be capable of broadening the absorption cross-section.[142]

5.7. Meta-Holography

Holography, as a revolutionary imaging technique that reconstructs electromagnetic waves by both amplitude and phase information, can be used for displaying and storing information. After the introduction of computer-generated holography (CGH), where holograms can be generated by digital computing and reconstructed by optics components, real objects are no longer needed to scatter electromagnetic radiation and the interference recording process. Conventional CGH adopts spatial light modulators (SLM) to reconfigure the phase retardation of light with liquid crystals and possesses a large pixel size. Since metasurfaces can be used to manipulate the polarization, phase, and amplitude of outgoing electromagnetic waves, they provide an excellent and compact platform for meta-holography applications.[144–146] Gerchberg-Saxton algorithms are often adopted to design the acquired phase distribution to transform a given input intensity distribution arriving at a hologram plane into a desired intensity distribution at the detection plane.[147]

Q. Wang et al. demonstrated all-dielectric meta-holograms with control over both phase and amplitude distribution and proved the superiority of their approach over traditional phase-only or amplitude-only modulation holograms, as shown in **Figure 10**, where meta-holography allows tailoring both the phase and amplitude of the virtual object and the hologram can be stretched and rotated along the propagating direction of the THz wave.[148] Other than improved resolution by reducing crosstalk, they also demonstrated that the holographic images can be shifted, stretched, and rotated along the longitudinal direction, giving more degrees of freedom for information storage.

5.8. Tunable Devices

Active components will play an important role in terahertz imaging and wireless communication systems in the near future. For conventional all-dielectric metamaterials, once the materials and geometrical parameters are selected, the electromagnetic responses are fixed. As a result, the tunability of all-dielectric metasurfaces could largely expand its usability and applicable fields.

Tuning metasurfaces can be implemented in either a mechanical way, i.e., changing the geometric features of the device, or through tuning the physical properties of the constituent materials in real time. Recent progress in adaptive control of propagating terahertz waves are based on modifying their terahertz response through mechanical,[153,154] optical,[15,155] electrical[156,157] or thermal stimuli.[154,158,159]

Microelectromechanical systems (MEMS) exploit piezoelectric and pyroelectric materials to enable dynamic control of the geometry of metamaterial devices and accordingly tune their electromagnetic response. A proof-of-concept work reported by K. Chen et al. theoretically designed and demonstrated a tunable reflective dielectric reflect-array consisting of lossless silicon pillars supported by a cyclic olefin copolymer (COC)[160–162] film and a metallic ground plane. As **Figure 11a** illustrated, by mechanically tuning the distance between the suspended silicon structures and the metallic film, the reflect array can attain efficient and switchable THz beam steering and focusing.[149]

Thermal stimuli can also be used to manipulate the device's response. VO_2, as a phase transition material, can be hybridized

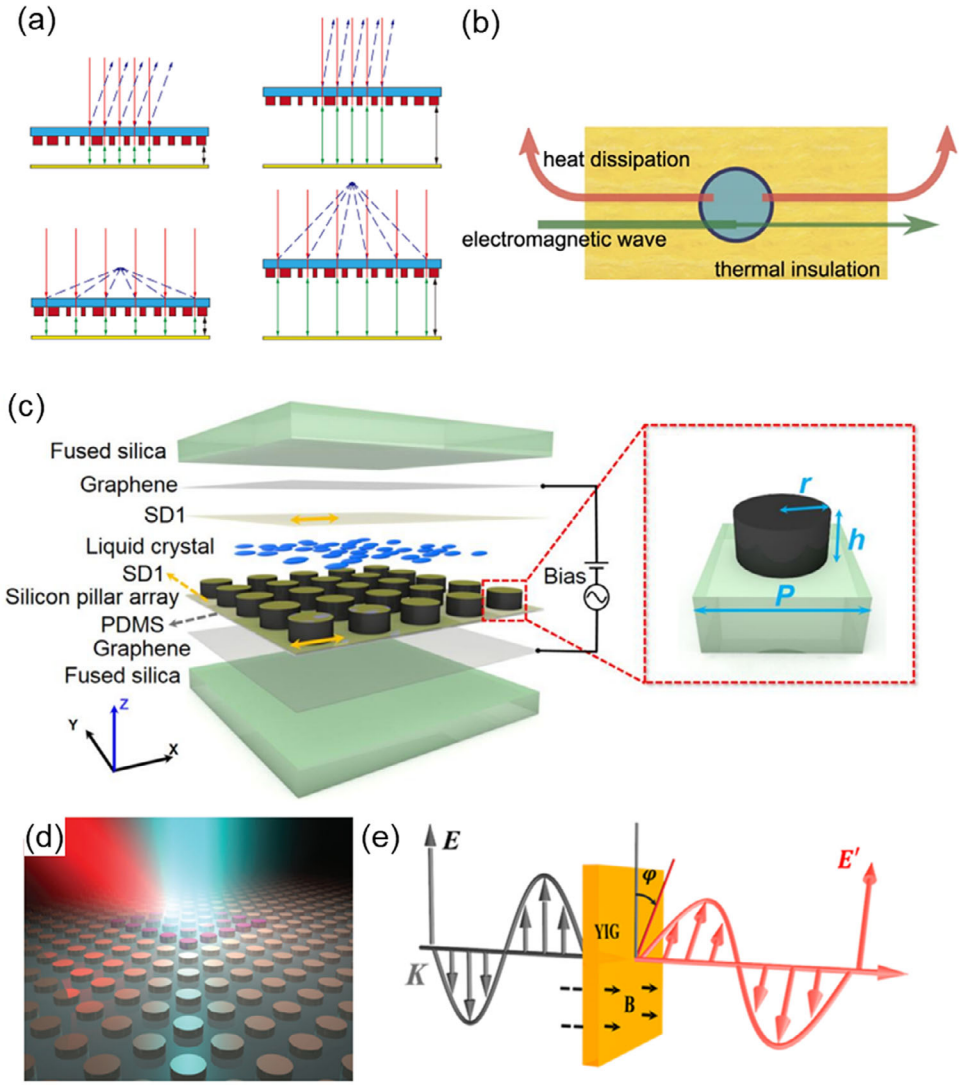

Figure 11. Tunable ADM devices. a) Switchable THz Beam Steering and Focusing via Mechanical Tuning. Reproduced with permission.[149] Copyright 2021, IEEE. b) Thermally Responsive Photonic Structures with Micro-Water Reservoirs. Reproduced with permission.[150] Copyright 2015, Springer Nature. c) Electro-Modulated Liquid Crystal and graphene ADM. Reproduced with permission.[42] Copyright 2018, MDPI. d) Optical photoexcitation modified ADM. Reproduced with permission.[151] Copyright 2018, WILEY-VCH Verlag GmbH & Co. KGaA. e) Magneto-optical modulated ADM. Reproduced with permission.[152] Copyright 2023, Optica Publishing Group.

within a metamaterial design to achieve tunability through thermal stimulus. Its drastic change between insulator and conductor states is exploited in THz switches and modulators. Similar to VO_2, the relative permittivity of $SrTiO_3$ can also be tuned by changing device temperature.[163] A. Andryieuski et al. theoretically discussed the possibility of a micro-water-reservoir (MWR) array to be used for realizing tunable all-dielectric photonic structures and metamaterials. In Figure 11b, the permittivity of water decreases as temperature increases so that the metamaterial made from it can be tuned by thermal stimuli at a slow speed. Its terahertz response can be manipulated by changing the elastic micro-water reservoir with mechanical force. If the MWR is partially filled, the metamaterial's electromagnetic properties can be tuned by the gravity-induced water redistribution.[150]

Electrical controls are also used to achieve the tunability of terahertz metamaterials.[119] Liquid crystals (LCs) possess large broadband birefringence and the ability to alter the local optical axis by an external electric field; they are good anisotropic material candidates for realizing electrically active tuning metamaterials at THz frequencies.[164,165] Metamaterial structures embedded inside LC cells have the molecules aligned in the direction of the applied electric field. L. Wang et al. developed a new LC with high-birefringence in the terahertz range and reduced the cell gap to achieve the required phase retardation, therefore reducing the device size, operating voltage, and response time.[166] To meet the request for transparent THz electrodes, few-layer porous graphene is adopted.[132] S Zhou et al. designed a tunable THz absorber. As shown in Figure 11c. Applying an electric field bias can change the orientation of liquid

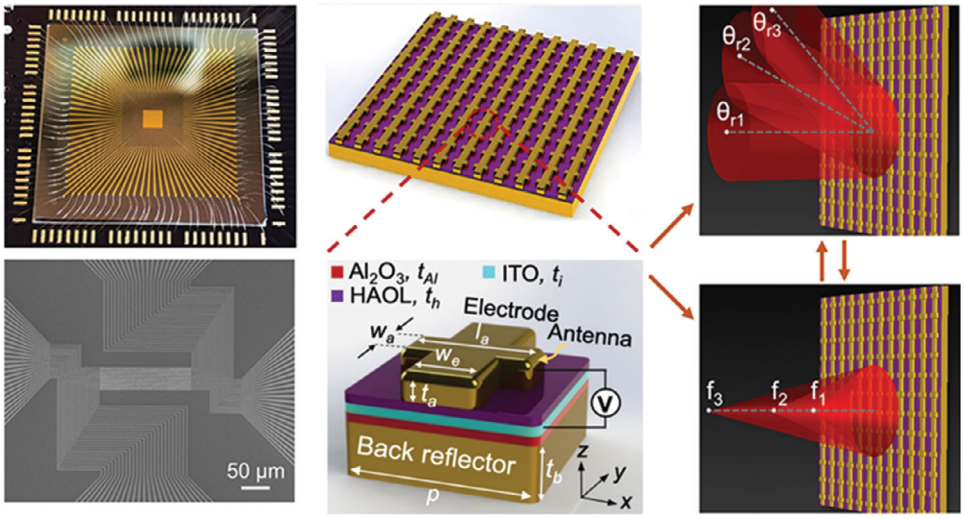

Figure 12. Programmable multifunctional metasurface, including photos, schematic of unit cell, and its demonstrations. Reproduced with permission.[189] Copy right 2020, American Chemical Society.

crystals, thereby modulating the optical response of the ADM. The overlap of electric and magnetic resonances of this material is broken due to the refractive index shift of the surrounding material (LC NJU-LDn-4). Thus, the absorption peak is separated into two peaks with lower intensity.[167] Zhao et al. integrate a LC layer with a silicon anisotropic metasurface. By adjusting the orientation of the LC relative to the silicon metasurface, the anisotropy of device can be effectively adjusted, which results in over 180° phase-shift range tunability. It open an avenue for effectively tuning and enhancing anisotropy and chirality of THz device.[168]

Graphene has interesting electronic and optical properties. Its optical parameters can be modulated by changing its Fermi energy. Therefore, it can be used to make actively tunable metamaterial.[169,170] This has been widely demonstrated in metallic metamaterials.[171,172] For ADM, L. Wang et al. demonstrated graphene can be used to adjust the electric field distribution on the metasurface and thus manipulate its electromagnetic response.[42] By placing graphene stripes under different regions of the dielectric resonators, the EIT-effect-based transmission peak gradually decreases by increasing the Fermi energy of graphene and shows different modulation depths.

Optical photoexcitation modifying the conductivity of a semiconductor through photocarrier generation is an effective way to modulate its electromagnetic response.[111,116] A. Berrier used a femtosecond laser as the optical pump to modulate undoped silicon's carrier's density, thus actively controlling the terahertz response of a bowtie antenna on picosecond timescale.[173] K. Fan et al. demonstrated a tunable transmission intensity Huygens' metasurface absorber through optical excitation as Figure 11d illustrated.[151] There, through modifying the magnetic dipole-like odd eigenmode to change critical coupled states, a large modulation depth of 99.93% and a phase change of $\pi/2$ at 1.03 THz was achieved. Besides, the highest modulation speed is 25 μs, and even down to sub-picosecond with material optimization is expected. Although this approach shows more flexibility and higher modulation speed compared to some other methods, it requires an intense external laser, which unavoidably increases the size of the device.

Magnetic field modulation is an effective adjusting approach for those materials whose refractive index are sensitive to external magnetic field, such as Yttrium Iron Garnet (YIG),[152,174,175] InSb,[176,177] and hexagonal ferrites,[178] etc. YIG, in particular, exhibits low loss in the THz regime.[174,175] As shown in Figure 11e, for a typical magneto-optical modulated ADMs, when linearly polarized light passes through YIG under a magnetic field, its polarization plane rotates which is so-called Faraday effect.[179,180] D Zhao et al. utilized the magneto-optical effects in YIG crystals to realize actively control of spin state of terahertz waves and terahertz beams steering. This non-reciprocal phase shift also enables device isolation for the reflected beam.[152]

5.9. Programmable Metasurfaces

Programmable metasurfaces represent an advanced engineering of tunable metasurface technologies. Based on the generalized Fresnel equations, real-time wavefront reshaping of incident waves can be realized through phase and amplitude control of each constituent unit of metasurface. Normally, phase differences and amplitude responses are discretized into through encoded electrical levels or optical control.[181–184] These codes are then processed into data arrays according to the desired waveform, thereby enabling programmability of the metasurface.[185–188] Ideally, phase of each unit can be tuned from 0 to 2π, and the higher the coding flexibility, the richer the functionalities of the programmable metasurfaces can have. **Figure 12** shows a fabricated a near-infrared programmable metasurface by Kafaie et al. The top layer-Indium Tin Oxide (ITO) is used as an electric contact for reference voltage, the dielectric constant of the dielectric constant of the hafnium/aluminum oxide nanolaminate (HAOL) can be independently tuned by vary the Direct Current (DC) bias beneath them, thus controlling the amplitude

and phase response of the elements to reflected waves, achieving beam control and dynamic focusing.[189] This method offers good compatibility for larger-sized programmable ADMs.

6. Outlook

As demonstrated above, with the mass production of metasurfaces-based terahertz devices, more attention should be paid to the fabrication process. To scale up the product manufacture, the bottleneck is how to enhance the yielding of low-loss polymer substrates and develop customized wafer bonding techniques.

Combining ADM with 2D materials is an intriguing and promising research direction. As mentioned in Section 1, 2D materials' properties depend on their Fermi energy or chemical potential, which can be manipulated by electrostatic or chemical doping. Therefore, by integrating single layers, multiple layers, or heterostructures of 2D materials into ADM, one can provide more degrees of freedom in designing new tunable metamaterials with advanced features. On the other hand, the coexistence of strong electric and magnetic resonances can reversely tune the electronic and magnetic properties of the 2D materials,[190] which is also promising for devices with active terahertz responses.

In fact, the etching process introduced the surface roughness and inhomogeneities can lead to dielectric losses which should is an unignorable factor to metasurface performance.[191,192] Metal behaves like perfect conductors in the terahertz band,[14] conventional dipole resonance modes have not shown a significant advantage dealing with the loss for all-dielectric materials.[14,193] The most definitive merit of all-dielectric materials lies in the ease of fabrication of the exchange of photonic angular momentum based three-dimensional resonant structures.[17,57,135,136] Thus, in order to diminish the ADMs loss, proper selection of materials with low loss,[58,71] applying resonant modes such as Bound States in the Continuum (BIC) and Fano resonances,[36,40,41,47,48] coating matching,[194] and improving the surface roughness and uniformity of samples are crucial approaches.

As we look to the future, the development of all-dielectric metasurfaces in the terahertz range will undoubtedly continue to push the boundaries of what is possible in various scientific and technological domains. In order to fully realize the potential of ADM-based devices, it is essential to foster interdisciplinary collaboration, bringing together expertise from different fields such as physics, materials science, engineering, and chemistry. Undoubtedly, this interdisciplinary approach will facilitate the discovery of novel materials, innovative fabrication techniques, and cutting-edge design methodologies, ultimately expanding the horizons of terahertz technology.

Furthermore, the integration of emerging technologies, such as machine learning, quantum materials, and metamaterial-inspired designs, will play a vital role in addressing current challenges and propelling the field toward new heights. By exploring the interplay between all-dielectric metasurfaces and these emerging technologies, researchers can uncover new possibilities and develop advanced terahertz devices with unprecedented capabilities.

In summary, all-dielectric metasurfaces represent a thriving and rapidly evolving research area with the potential to revolutionize a broad spectrum of industries and scientific disciplines. By embracing interdisciplinary collaboration and leveraging cutting-edge technologies, the future of ADM-based terahertz devices is poised for growth, innovation, and far-reaching impact. As researchers continue to explore and push the boundaries of this promising field, the applications and implications of all-dielectric metasurfaces in the terahertz range will become increasingly diverse and transformative.

Acknowledgements

This work was supported by the National Key R&D Program of China (2022YFC3006303).

Conflict of Interest

The authors declare no conflict of interest.

Author Contributions

D.H. performed investigation; data curation; formal analysis; wrote the – original draft; J.L. performed investigation; data curation; P.Z., Y,Z. performed investigation. R.M. wrote-review and edited the original draft. L.M. performed supervision, funding acquisition, conceptualization, formal analysis, wrote –review and edited the original drafft.

Received: November 20, 2023
Revised: March 19, 2024
Published online:

[1] M. Tonouchi, *Nat. Photonics* **2007**, *1*, 97.
[2] Z. Chen, X. Ma, B. Zhang, Y. Zhang, Z. Niu, N. Kuang, W. Chen, L. Li, S. Li, *Chin. Commun.* **2019**, *16*, 1.
[3] T. Nagatsuma, G. Ducournau, C. C. Renaud, *Nat. Photonics* **2016**, *10*, 371.
[4] X. Yan, M. Yang, Z. Zhang, L. Liang, D. Wei, M. Wang, M. Zhang, T. Wang, L. Liu, J. Xie, J. Yao, *Biosens. Bioelectron.* **2019**, *126*, 485.
[5] K. Su, Y.-C. Shen, J. A. Zeitler, *IEEE Trans. Terahertz Sci. Technol.* **2014**, *4*, 432.
[6] Y. H. Tao, A. J. Fitzgerald, V. P. Wallace, *Sensors* **2020**, *20*, 712.
[7] C. G. Wade, N. Šibalić, N. R. de Melo, J. M. Kondo, C. S. Adams, K. J. Weatherill, *Nat. Photonics* **2016**, *11*, 40.
[8] C. Jansen, S. Wietzke, O. Peters, M. Scheller, N. Vieweg, M. Salhi, N. Krumbholz, C. Jordens, T. Hochrein, M. Koch, *Appl. Opt.* **2010**, *49*, E48.
[9] J. Pan, H. Hu, Z. Li, J. Mu, Y. Cai, H. Zhu, *Nanoscale Advances* **2021**, *3*, 1515.
[10] S. Venkatachalam, K. Zeranska-Chudek, M. Zdrojek, D. Hourlier, *Nano Select* **2020**, *1*, 471.
[11] Y. Wang, D. Zhu, Z. Cui, L. Hou, L. Lin, F. Qu, X. Liu, P. Nie, *ACS Omega* **2019**, *4*, 18645.
[12] W. Cen, T. Lang, J. Wang, M. Xiao, *Appl. Surf. Sci.* **2022**, *575*, 151723.
[13] W. Shi, F. Fan, S. Li, Z. Zhang, H. Liu, X. Wang, S. Chang, *Sens. Actuators, B* **2022**, *362*, 131777.
[14] J. A. Álvarez-Sanchis, B. Vidal, S. A. Tretyakov, A. Díaz-Rubio, *Phys. Rev. Appl.* **2023**, *19*, 014009.
[15] C. Lan, H. Ma, M. Wang, Z. Gao, K. Liu, K. Bi, J. Zhou, X. Xin, *ACS Appl. Mater. Interfaces* **2019**, *11*, 14229.
[16] Z. G. Wang, Y. Q. Zhou, L. M. Yang, C. Gong, *J. Phys. D: Appl. Phys.* **2017**, *50*, 375107.

[17] W. Shi, F. Fan, Z. Zhang, T. Zhang, S. Li, X. Wang, S. Chang, *Appl. Sci.* **2021**, *11*, 8892.
[18] D. R. Smith, W. J. Padilla, D. C. Vier, S. C. Nemat-Nasser, S. Schultz, *Phys. Rev. Lett.* **2000**, *84*, 4184.
[19] V. M. Shalaev, *Nat. Photonics* **2007**, *1*, 41.
[20] I. Bernardeschi, M. Ilyas, L. Beccai, *Adv. Intell. Syst.* **2021**, *3*, 2100051.
[21] L. Wu, K. Cheng, Y.-S. Lin, *Results Phys.* **2022**, *43*, 106092.
[22] D. V. Bochek, K. B. Samusev, D. A. Yavsin, M. V. Zhukov, M. F. Limonov, M. V. Rybin, I. I. Shishkin, A. D. Sinelnik, *Opt. Laser Technol.* **2021**, *141*, 107124.
[23] N. Meinzer, W. L. Barnes, I. R. Hooper, *Nat. Photonics* **2014**, *8*, 889.
[24] S. Jahani, Z. Jacob, *Nat. Nanotechnol.* **2016**, *11*, 23.
[25] A. Arbabi, Y. Horie, M. Bagheri, A. Faraon, *Nat. Nanotechnol.* **2015**, *10*, 937.
[26] A. Krasnok, S. Makarov, M. Petrov, R. Savelev, P. Belov, Y. Kivshar, *SPIE* **2015**, *9502*, 950203.
[27] Q. Zhao, J. Zhou, F. Zhang, D. Lippens, *Mater. Today* **2009**, *12*, 60.
[28] S. Kruk, Y. Kivshar, *ACS Photonics* **2017**, *4*, 2638.
[29] D. Tzarouchis, A. Sihvola, *Appl. Sci.* **2018**, *8*, 184.
[30] M. Decker, I. Staude, M. Falkner, J. Dominguez, D. N. Neshev, I. Brener, T. Pertsch, Y. S. Kivshar, *Adv. Opt. Mater.* **2015**, *3*, 813.
[31] Q. Zhao, L. Kang, B. Du, H. Zhao, Q. Xie, X. Huang, B. Li, J. Zhou, L. Li, *Phys. Rev. Lett.* **2008**, *101*, 027402.
[32] I. Staude, J. Schilling, *Nat. Photonics* **2017**, *11*, 274.
[33] Y. H. Fu, A. I. Kuznetsov, A. E. Miroshnichenko, Y. F. Yu, B. Luk'yanchuk, *Nat. Commun.* **2013**, *4*, 1527.
[34] J. He, T. Dong, B. Chi, Y. Zhang, *J. Infrared Millim.Terahertz Waves* **2020**, *41*, 607.
[35] T. Ma, Q. Huang, H. He, Y. Zhao, X. Lin, Y. Lu, *Opt. Express* **2019**, *27*, 16624.
[36] B. Luk'yanchuk, N. I. Zheludev, S. A. Maier, N. J. Halas, P. Nordlander, H. Giessen, C. T. Chong, *Nat. Mater.* **2010**, *9*, 707.
[37] M. V. Rybin, K. B. Samusev, A. N. Poddubny, A. Hosseinzadeh, E. Semouchkina, G. Semouchkin, Y. S. Kivshar, M. F. Limonov, 7th Inthernational Congress on Advanced Electromagnetic Meterials in Microwaves and Optics **2013**, 226.
[38] V. A. Fedotov, M. Rose, S. L. Prosvirnin, N. Papasimakis, N. I. Zheludev, *Phys. Rev. Lett.* **2007**, *99*, 147401.
[39] X. He, F. Liu, F. Lin, W. Shi, *Optics Express* **2019**, *27*, 13831.
[40] M. F. Limonov, M. V. Rybin, A. N. Poddubny, Y. S. Kivshar, *Nat. Photonics* **2017**, *11*, 543.
[41] G. Cao, S. Dong, L. M. Zhou, Q. Zhang, Y. Deng, C. Wang, H. Zhang, Y. Chen, C. W. Qiu, X. Liu, *Adv. Opt. Mater.* **2020**, *8*, 1902153.
[42] S. Zhou, Z. Shen, R. Kang, S. Ge, W. Hu, *Appl. Sci.* **2018**, *8*, 2211.
[43] X. Chen, W. Fan, *Nanomaterials* **2020**, *10*, 623.
[44] S. Han, P. Pitchappa, W. Wang, Y. K. Srivastava, M. V. Rybin, R. Singh, *Adv. Opt. Mater.* **2021**, 9, 2002001.
[45] S. Han, M. V. Rybin, P. Pitchappa, Y. K. Srivastava, Y. S. Kivshar, R. Singh, *Adv. Opt. Mater.* **2019**, *8*, 1900959.
[46] S. Joseph, S. Pandey, S. Sarkar, J. Joseph, *Nanophotonics* **2021**, *10*, 4175.
[47] S. Han, L. Cong, Y. K. Srivastava, B. Qiang, M. V. Rybin, A. Kumar, R. Jain, W. X. Lim, V. G. Achanta, S. S. Prabhu, Q. J. Wang, Y. S. Kivshar, R. Singh, *Adv. Mater.* **2019**, *31*, 1901921.
[48] W. Wang, Y. K. Srivastava, T. C. Tan, Z. Wang, R. Singh, *Nat. Commun.* **2023**, *14*, 2811.
[49] M. Kenney, S. Li, X. Zhang, X. Su, T. T. Kim, D. Wang, D. Wu, C. Ouyang, J. Han, W. Zhang, H. Sun, S. Zhang, *Adv. Mater.* **2016**, *28*, 9567.
[50] Z. Gao, S. Golla, R. Sawant, V. Osipov, G. Briere, S. Vezian, B. Damilano, P. Genevet, K. E. Dorfman, *Nanophotonics* **2020**, *9*, 4711.
[51] S. Chang, X. Guo, X. Ni, *Annu. Rev. Mater. Res.* **2018**, *48*, 279.
[52] E. Hasman, V. Kleiner, G. Biener, A. Niv, *Opt. Photon. News* **2002**, *13*, 45.
[53] F. Yue, D. Wen, J. Xin, B. D. Gerardot, J. Li, X. Chen, *ACS. Photonics* **2016**, *3*, 1558.
[54] L. Huang, X. Chen, H. Muhlenbernd, G. Li, B. Bai, Q. Tan, G. Jin, T. Zentgraf, S. Zhang, *Nano Lett.* **2012**, *12*, 5750.
[55] S. Wang, X. Wang, Q. Kan, J. Ye, S. Feng, W. Sun, P. Han, S. Qu, Y. Zhang, *Opt. Express* **2015**, *23*, 26434.
[56] H. Zhang, X. Zhang, Q. Xu, C. Tian, Q. Wang, Y. Xu, Y. Li, J. Gu, Z. Tian, C. Ouyang, X. Zhang, C. Hu, J. Han, W. Zhang, *Adv. Opt. Mater.* **2018**, *6*, 1700773.
[57] R. T. Ako, A. Upadhyay, W. Withayachumnankul, M. Bhaskaran, S. Sriram, *Adv. Opt. Mater.* **2019**, *8*, 1900750.
[58] X. Liu, Z. Ren, T. Yang, L. Chen, Q. Wang, J. Zhou, *J. Mater. Sci. Technol.* **2021**, *62*, 249.
[59] Y. Zhao, B. Li, C. Lan, K. Bi, Z. Qu, *Opt. Express* **2017**, *25*, 22158.
[60] P. Zhu, W. Yang, R. Wang, S. Gao, B. Li, Q. Li, *Adv. Opt. Mater.* **2017**, *5*, 7.
[61] A. Karvounis, F. Timpu, V. V. Vogler-Neuling, R. Savo, R. Grange, *Adv. Opt. Mater.* **2020**, *8*, 2001249.
[62] L. Wu, L. Jiang, C. Ding, Q. Sheng, X. Ding, J. Yao, J. Infrared, *J. Infrared Millim. Terahertz Waves* **2014**, *36*, 1.
[63] L. Wu, J. Liu, H. Li, C. Ding, N. Xu, X. Zhao, Z. Xu, Q. Sheng, J. Yao, J. Li, X. Ding, W. Zhang, *Sci. Rep.* **2017**, *7*, 6072.
[64] L. Wu, H. Li, L. Jiang, C. Ding, Q. Sheng, X. Ding, J. Yao, *Opt. Mater. Express* **2014**, *4*, 2595.
[65] A. Podzorov, G. Gallot, *Appl. Opt.* **2008**, *47*, 3254.
[66] K. Fan, J. Y. Suen, X. Liu, W. J. Padilla, *Optica* **2017**, *4*, 601.
[67] P. D. Cunningham, N. N. Valdes, F. A. Vallejo, L. M. Hayden, B. Polishak, X.-H. Zhou, J. Luo, A. K. Y. Jen, J. C. Williams, R. J. Twieg, *J. Appl. Phys.* **2011**, *109*, 043505.
[68] S. Walia, C. M. Shah, P. Gutruf, H. Nili, D. R. Chowdhury, W. Withayachumnankul, M. Bhaskaran, S. Sriram, *Appl. Phys. Rev.* **2015**, *2*, 011303.
[69] X. Liu, S. MacNaughton, D. B. Shrekenhamer, H. Tao, S. Selvarasah, A. Totachawattana, R. D. Averitt, M. R. Dokmeci, S. Sonkusale, W. J. Padilla, *Appl. Phys. Lett.* **2010**, *96*, 1.
[70] F. Pavanello, F. Garet, M.-B. Kuppam, E. Peytavit, M. Vanwolleghem, F. Vaurette, J.-L. Coutaz, J.-F. Lampin, *Appl. Phys. Lett.* **2013**, *102*, 11.
[71] X. Liu, Z. Ren, T. Yang, Y. Hao, Q. Wang, J. Zhou, *Scr. Mater.* **2020**, *184*, 30.
[72] Y. Yang, B. Cui, Z. Geng, S. Feng, *Appl. Phys. Lett.* **2015**, *106*, 11.
[73] H. Němec, P. Kužel, F. Kadlec, C. Kadlec, R. Yahiaoui, P. Mounaix, *Phys. Rev. B* **2009**, *79*, 241108.
[74] H. Němec, C. Kadlec, F. Kadlec, P. Kužel, R. Yahiaoui, U. C. Chung, C. Elissalde, M. Maglione, P. Mounaix, *Appl. Phys. Lett.* **2012**, *100*, 061117.
[75] K. Bi, D. Yang, J. Chen, Q. Wang, H. Wu, C. Lan, Y. Yang, *Photon. Res.* **2019**, *7*, 457.
[76] D. Yang, C. Zhang, X. Ju, Y. Ji, C. Lan, *Opt. Express* **2020**, *28*, 2547.
[77] C. Qu, E. C. Kinzel, *Opt. Lett.* **2016**, *41*, 3399.
[78] P. J. P. Chausse, E. D. Le Boulbar, S. D. Lis, P. A. Shields, *Opt. Express* **2019**, *27*, 5918.
[79] D. Andrén, J. Martínez-Llinàs, P. Tassin, M. Käll, R. Verre, *ACS Photonics* **2020**, *7*, 885.
[80] Y. Sin Tan, H. Wang, H. Wang, C. Pan, J. K. W. Yang, *Photon. Res.* **2023**, *11*, B103.
[81] C. Li, P. Yu, Y. Huang, Q. Zhou, J. Wu, Z. Li, X. Tong, Q. Wen, H.-C. Kuo, Z. M. Wang, *Prog. Surf. Sci.* **2020**, *95*, 100584.
[82] X. Liu, K. Fan, I. V. Shadrivov, W. J. Padilla, *Opt. Express* **2017**, *25*, 191.
[83] L. Deng, J. Teng, H. Liu, Q. Y. Wu, J. Tang, X. Zhang, S. A. Maier, K. P. Lim, C. Y. Ngo, S. F. Yoon, S. J. Chua, *Adv. Opt. Mater.* **2013**, *1*, 128.
[84] S. An, C. Fowler, B. Zheng, M. Y. Shalaginov, H. Tang, H. Li, L. Zhou, J. Ding, A. M. Agarwal, C. Rivero-Baleine, K. A. Richardson, T. Gu, J. Hu, H. Zhang, *ACS Photonics* **2019**, *6*, 3196.

[85] C. C. Nadell, B. Huang, J. M. Malof, W. J. Padilla, *Opt. Express* **2019**, *27*, 27523.
[86] Y. Deng, S. Ren, K. Fan, J. M. Malof, W. J. Padilla, *Opt. Express* **2021**, *29*, 7526.
[87] J. Cheng, R. Li, Y. Wang, Y. Yuan, X. Wang, S. Chang, *Opt. Laser Technol.* **2023**, *159*, 109038.
[88] J. Wang, Z. Lin, Y. Fan, L. Mei, W. Deng, J. Lv, Z. Xu, *Materials* **2022**, *15*, 7008.
[89] S. An, B. Zheng, H. Tang, M. Y. Shalaginov, L. Zhou, H. Li, M. Kang, K. A. Richardson, T. Gu, J. Hu, C. Fowler, H. Zhang, *Adv. Opt. Mater.* **2021**, *9*, 2001433.
[90] M. M. R. Elsawy, S. Lanteri, R. Duvigneau, J. A. Fan, P. Genevet, *Laser Photonics Rev.* **2020**, *14*, 1900445.
[91] Y. Zhao, X. Cao, J. Gao, Y. Sun, H. Yang, X. Liu, Y. Zhou, T. Han, W. Chen, *Sci. Rep.* **2016**, *6*, 23896.
[92] H. Ma, W. Zhang, *Optik* **2019**, *182*, 233.
[93] Q. Yuan, H. Ma, S. Sui, J. Wang, Y. Meng, Y. Pang, S. Qu, *J. Phys. D: Appl. Phys.* **2021**, *54*, 135001.
[94] J. Yang, J. A. Fan, *Opt. Lett.* **2017**, *42*, 3161.
[95] T. Phan, D. Sell, E. W. Wang, S. Doshay, K. Edee, J. Yang, J. A. Fan, *Light, Sci. Appl.* **2019**, *8*, 48.
[96] J. A. Fan, *MRS Bull.* **2020**, *45*, 196.
[97] Y. Zhao, M. Zhang, A. Alabastri, P. Nordlander, *ACS Nano* **2022**, *16*, 18951.
[98] A. K. González-Alcalde, R. Salas-Montiel, V. Kalt, S. Blaize, D. Macías, *Opt. Lett.* **2020**, *45*, 89.
[99] Y. Chen, Z. Ding, M. Zhang, J. Zhou, M. Li, M. Zhao, J. Wang, *Appl. Opt.* **2021**, *60*, 9200.
[100] D. Z. Zhu, E. B. Whiting, S. D. Campbell, D. B. Burckel, D. H. Werner, *ACS Photonics* **2019**, *6*, 2741.
[101] M. Naftaly, R. Dudley, *Appl. Opt.* **2011**, *50*, 3201.
[102] N. Krumbholz, K. Gerlach, F. Rutz, M. Koch, R. Piesiewicz, T. Kürner, D. Mittleman, *Appl. Phys. Lett.* **2006**, *88*, 202905.
[103] B. Slovick, Z. G. Yu, M. Berding, S. Krishnamurthy, *Phys. Rev. B* **2013**, *88*, 165116.
[104] P. Moitra, B. A. Slovick, Z. Gang Yu, S. Krishnamurthy, J. Valentine, *Appl. Phys. Lett.* **2014**, *104*, 17.
[105] Z. Song, Q. Chu, W. Wang, L. Ye, G. Cai, Q. H. Liu, *Europhys. Lett.* **2017**, *119*, 47004.
[106] B. Fang, C. Li, Y. Peng, X. Jing, *Microwave Opt. Technol. Lett.* **2019**, *61*, 1634.
[107] L. Jiang, B. Fang, Z. Yan, C. Li, H. Gan, Y. He, Z. Hong, X. Jing, *Microelectron. Eng.* **2020**, *223*, 111216.
[108] P. Yu, L. V. Besteiro, Y. Huang, J. Wu, L. Fu, H. H. Tan, C. Jagadish, G. P. Wiederrecht, A. O. Govorov, Z. Wang, *Adv. Opt. Mater.* **2018**, *7*, 1800995.
[109] V. A. Fedotov, A. V. Rogacheva, N. I. Zheludev, P. L. Mladyonov, S. L. Prosvirnin, *Appl. Phys. Lett.* **2006**, *88*, 091119.
[110] D. Headland, S. Nirantar, W. Withayachumnankul, P. Gutruf, D. Abbott, M. Bhaskaran, C. Fumeaux, S. Sriram, *Adv. Mater.* **2015**, *27*, 7137.
[111] Y. Jiao, J. Lou, Z. Ma, L. Cong, X. Xu, B. Zhang, D. Li, Y. Yu, W. Sun, Y. Yan, S. Hu, B. Liu, Y. Huang, L. Sun, R. Wang, R. Singh, Y. Fan, C. Chang, X. Du, *Mater. Horiz.* **2022**, *9*, 2984.
[112] D. Headland, Y. Monnai, D. Abbott, C. Fumeaux, W. Withayachumnankul, *APL Photonics* **2018**, *3*, 051101.
[113] D. Headland, T. Niu, E. Carrasco, D. Abbott, S. Sriram, M. Bhaskaran, C. Fumeaux, W. Withayachumnankul, *IEEE J. Sel. Top. Quantum Electron.* **2017**, *23*, 1.
[114] N. Yu, P. Genevet, M. A. Kats, F. Aieta, J. P. Tetienne, F. Capasso, Z. Gaburro, *Science* **2011**, *334*, 333.
[115] N. K. Grady, J. E. Heyes, D. R. Chowdhury, Y. Zeng, M. T. Reiten, A. K. Azad, A. J. Taylor, D. A. Dalvit, H. T. Chen, *Science* **2013**, *340*, 1304.
[116] R. Yang, Y. Fan, W. Zhu, C. Hu, S. Chen, H. Wei, W. Chen, C. T. Chan, Q. Zhao, J. Zhou, F. Zhang, C. W. Qiu, *Laser Photonics Rev.* **2023**, *17*, 2200975.
[117] D. Headland, E. Carrasco, S. Nirantar, W. Withayachumnankul, P. Gutruf, J. Schwarz, D. Abbott, M. Bhaskaran, S. Sriram, J. Perruisseau-Carrier, C. Fumeaux, *ACS. Photonics* **2016**, *3*, 1019.
[118] Z. Ma, S. M. Hanham, P. Albella, B. Ng, H. T. Lu, Y. Gong, S. A. Maier, M. Hong, *ACS. Photonics* **2016**, *3*, 1010.
[119] R. Yang, F. Zhang, Z. Li, Q. Fu, Y. Fan, *Opt. Laser Technol.* **2023**, *163*, 109380.
[120] M. Khorasaninejad, F. Capasso, *Science* **2017**, *358*, 6367.
[121] N. Yu, F. Capasso, *Nat. Mater.* **2014**, *13*, 139.
[122] W. Liu, A. E. Miroshnichenko, D. N. Neshev, Y. S. Kivshar, *ACS Nano* **2012**, *6*, 5489.
[123] M. Zhao, M. K. Chen, Z. P. Zhuang, Y. Zhang, A. Chen, Q. Chen, W. Liu, J. Wang, Z. M. Chen, B. Wang, X. Liu, H. Yin, S. Xiao, L. Shi, J. W. Dong, J. Zi, D. P. Tsai, *Light, Sci.Appl.* **2021**, *10*, 52.
[124] D. Jia, Y. Tian, W. Ma, X. Gong, J. Yu, G. Zhao, X. Yu, *Opt. Lett.* **2017**, *42*, 4494.
[125] Q. Cheng, M. Ma, D. Yu, Z. Shen, J. Xie, J. Wang, N. Xu, H. Guo, W. Hu, S. Wang, T. Li, S. Zhuang, *Sci. Bull.* **2019**, *64*, 1525.
[126] X. Jiang, H. Chen, Z. Li, H. Yuan, L. Cao, Z. Luo, K. Zhang, Z. Zhang, Z. Wen, L. G. Zhu, X. Zhou, G. Liang, D. Ruan, L. Du, L. Wang, G. Chen, *Opt. Express* **2018**, *26*, 14132.
[127] D. Wang, S. Sun, Z. Feng, W. Tan, *Nanoscale Res. Lett.* **2021**, *16*, 157.
[128] H. Zhang, X. Zhang, Q. Xu, Q. Wang, Y. Xu, M. Wei, Y. Li, J. Gu, Z. Tian, C. Ouyang, X. Zhang, C. Hu, J. Han, W. Zhang, *Photon. Res.* **2017**, *6*, 24.
[129] Y. Hu, X. Wang, X. Luo, X. Ou, L. Li, Y. Chen, Y. Ping, S. Wang, H. Duan, *Nanophotonics* **2020**, *9*, 3755.
[130] J. Zi, Q. Xu, Q. Wang, C. Tian, Y. Li, X. Zhang, J. Han, W. Zhang, *Appl. Phys. Lett.* **2018**, *113*, 101104.
[131] W. S. L. Lee, R. T. Ako, M. X. Low, M. Bhaskaran, S. Sriram, C. Fumeaux, W. Withayachumnankul, *Optics Express* **2018**, *26*, 14392.
[132] S. Ge, P. Chen, Z. Shen, W. Sun, X. Wang, W. Hu, Y. Zhang, Y. Lu, *Opt. Express* **2017**, *25*, 12349.
[133] R. C. Devlin, A. Ambrosio, N. A. Rubin, J. P. B. Mueller, F. Capasso, *Science* **2017**, *358*, 896.
[134] L. Marrucci, C. Manzo, D. Paparo, *Phys. Rev. Lett.* **2006**, *96*, 163905.
[135] Y. Xu, H. Zhang, Q. Li, X. Zhang, Q. Xu, W. Zhang, C. Hu, X. Zhang, J. Han, W. Zhang, *Nanophotonics* **2020**, *9*, 3393.
[136] C. Zheng, J. Li, G. Wang, J. Li, S. Wang, M. Li, H. Zhao, Z. Yue, Y. Zhang, Y. Zhang, J. Yao, *Nanophotonics* **2021**, *10*, 1347.
[137] M. Kenney, J. Grant, Y. D. Shah, I. Escorcia-Carranza, M. Humphreys, D. R. S. Cumming, *ACS Photonics* **2017**, *4*, 2604.
[138] M. A. Cole, D. A. Powell, I. V. Shadrivov, *Nanotechnology* **2016**, *27*, 424003.
[139] L.-H. Du, J. Li, Z.-H. Zhai, K. Meng, Q. Liu, S.-C. Zhong, P.-W. Zhou, L.-G. Zhu, Z.-R. Li, Q.-X. Peng, *AIP Adv.* **2016**, *6*, 055112.
[140] M. Pu, M. Wang, C. Hu, C. Huang, Z. Zhao, Y. Wang, X. Luo, *Opt. Express* **2012**, *20*, 25513.
[141] H. Liu, K. Luo, S. Tang, D. Peng, F. Hu, L. Tu, *Materials* **2018**, *11*, 2590.
[142] S. M. Hanham, A. I. Fernandez-Dominguez, J. H. Teng, S. S. Ang, K. P. Lim, S. F. Yoon, C. Y. Ngo, N. Klein, J. B. Pendry, S. A. Maier, *Adv. Mater.* **2012**, *24*, OP226.
[143] W. Withayachumnankul, C. M. Shah, C. Fumeaux, B. S. Y. Ung, W. J. Padilla, M. Bhaskaran, D. Abbott, S. Sriram, *ACS Photonics* **2014**, *1*, 625.

[144] L. Wang, S. Kruk, H. Tang, T. Li, I. Kravchenko, D. N. Neshev, Y. S. Kivshar, *Optica* **2016**, *3*, 1504.
[145] X. Ni, A. V. Kildishev, V. M. Shalaev, *Nat. Commun.* **2013**, *4*, 2807.
[146] W. Wan, J. Gao, X. Yang, *Adv. Opt. Mater.* **2017**, *5*, 1700541.
[147] A. Siemion, J. Infrared, *J. Infrared Millim. Terahertz Waves* **2019**, *40*, 477.
[148] Q. Wang, Q. Xu, X. Zhang, C. Tian, Y. Xu, J. Gu, Z. Tian, C. Ouyang, X. Zhang, J. Han, W. Zhang, *ACS Photonics* **2017**, *5*, 599.
[149] K. Chen, X. Zhang, X. Chen, T. Wu, Q. Wang, Z. Zhang, Q. Xu, J. Han, W. Zhang, *IEEE Photon. J.* **2021**, *13*, 1.
[150] A. Andryieuski, S. M. Kuznetsova, S. V. Zhukovsky, Y. S. Kivshar, A. V. Lavrinenko, *Sci. Rep.* **2015**, *5*, 13535.
[151] K. Fan, J. Zhang, X. Liu, G. F. Zhang, R. D. Averitt, W. J. Padilla, *Adv. Mater.* **2018**, *30*, 1800278.
[152] D. Zhao, F. Fan, J. Liu, Z. Tan, H. Wang, Q. Yang, Q. Wen, S. Chang, *Optica* **2023**, *10*, 1295.
[153] C. Zhang, J. Jing, Y. Wu, Y. Fan, W. Yang, S. Wang, Q. Song, S. Xiao, *ACS Nano* **2020**,*14*, 1418.
[154] S. Peng, X. Lu, L. Tang, X. Chang, J. Yan, Q. Shi, K. Chen, J. Li, L. Du, W. Huang, *Optics Express* **2023**, *31*, 2644.
[155] Y.-H. Shih, X.-Y. Lin, H. M. Silalahi, C.-R. Lee, C.-Y. Huang, *Crystals* **2021**, *11*, 1100.
[156] J. Shi, H. Gao, X. Jia, L. Tang, X. Li, H. Ma, X. Li, H. Bai, X. Wang, P. Niu, J. Yao, *ACS Appl. Mater. Interfaces* **2022**, *14*, 55174.
[157] P. C. Wu, R. A. Pala, G. Kafaie Shirmanesh, W. H. Cheng, R. Sokhoyan, M. Grajower, M. Z. Alam, D. Lee, H. A. Atwater, *Nat. Commun.* **2019**, *10*, 3654.
[158] M. Rahmani, L. Xu, A. E. Miroshnichenko, A. Komar, R. Camacho-Morales, H. Chen, Y. Zárate, S. Kruk, G. Zhang, D. N. Neshev, Y. S. Kivshar, *Adv. Funct. Mater.* **2017**, *27*, 1700580.
[159] H. Luo, Y. Cheng, *Opt. Mater.* **2020**, *102*, 109801.
[160] L. M. Diaz-Albarran, E. Lugo-Hernandez, E. Ramirez-Garcia, M. A. Enciso-Aguilar, D. Valdez-Perez, P. Cereceda-Company, D. Granados, J. L. Costa-Krämer, *Microelectron. Eng.* **2018**, *191*, 84.
[161] H. S. Bark, M. W. Park, I. H. Baek, K. H. Jang, Y. U. Jeong, K. Lee, T. I. Jeon, *Opt. Express* **2022**, *30*, 7976.
[162] L. Cai, Z. H. Jiang, J. B. Wu, H. Chen, W. Hong, *Opt. Express* **2023**, *31*, 21706.
[163] X. He, F. Lin, F. Liu, W. Shi, *J. Phys. D: Appl. Phys.* **2020**, *53*, 155105.
[164] L. Wang, S. Ge, W. Hu, M. Nakajima, Y. Lu, *Opt. Mater. Express* **2017**, *7*, 2023.
[165] M. P. Hokmabadi, A. Tareki, E. Rivera, P. Kung, R. G. Lindquist, S. M. Kim, *AIP Adv.* **2017**, *7*, 015102.
[166] L. Wang, X.-W. Lin, W. Hu, G.-H. Shao, P. Chen, L.-J. Liang, B.-B. Jin, P.-H. Wu, H. Qian, Y.-N. Lu, X. Liang, Z.-G. Zheng, Y.-Q. Lu, *Light: Sci. Appl.* **2015**, *4*, e253.
[167] S. Zhou, Z. Shen, R. Kang, S. Ge, W. Hu, *Appl. Sci.* **2018**, *8*, 2211.
[168] J. Li, C. Zheng, J. Li, G. Wang, J. Liu, Z. Yue, X. Hao, Y. Yang, F. Li, T. Tang, Y. Zhang, Y. Zhang, J. Yao, *Photon. Res.* **2021**, *9*, 1939.
[169] S. Arezoomandan, H. Condori Quispe, A. Chanana, P. Gopalan, S. Banerji, A. Nahata, B. Sensale-Rodriguez, *Semicond. Sci. Technol.* **2018**, *33*, 104007.
[170] Y. Fan, N.-H. Shen, F. Zhang, Q. Zhao, Z. Wei, P. Zhang, J. Dong, Q. Fu, H. Li, C. M. Soukoulis, *ACS Photonics* **2018**, *5*, 1612.
[171] S. H. Lee, M. Choi, T. T. Kim, S. Lee, M. Liu, X. Yin, H. K. Choi, S. S. Lee, C. G. Choi, S. Y. Choi, X. Zhang, B. Min, *Nat. Mater.* **2012**, *11*, 936.
[172] S. Arezoomandan, H. O. Condori Quispe, N. Ramey, C. A. Nieves, B. Sensale-Rodriguez, *Carbon* **2017**, *112*, 177.
[173] A. Berrier, R. Ulbricht, M. Bonn, J. G. Rivas, *Opt. Express* **2010**, *18*, 23226.
[174] Y. L. Li, T. F. Li, Q. Y. Wen, F. Fan, Q. H. Yang, S. J. Chang, *Optics Express* **2020**, 21062.
[175] Y. L. Li, D. Zhang, M. Luo, Q. H. Yang, F. Fan, S. J. Chang, Q. Y. Wen, *OpticExpress* **2021**, *29*, 23540.
[176] J. Chochol, K. Postava, M. Čada, M. Vanwolleghem, L. Halagačka, J.-F. Lampin, J. Pištora, *AIP Adv.* **2016**, 6.
[177] H. Jing, Y. Wei, J. Duan, J. Hao, W. Zhao, Z. Qu, J. Wang, B. Zhang, *Opt. Mater.* **2022**, *129*, 112311.
[178] A. N. Grebenchukov, V. I. Ivanova, G. I. Kropotov, M. K. Khodzitsky, *Appl. Phys. Lett.* **2021**, *118*, 191104.
[179] B. Fan, M. E. Nasir, L. H. Nicholls, A. V. Zayats, V. A. Podolskiy, *Adv. Opt. Mater.* **2019**, 7, 1801420.
[180] S. Xia, D. O. Ignatyeva, Q. Liu, J. Qin, T. Kang, W. Yang, Y. Chen, H. Duan, L. Deng, D. Long, M. Veis, V. I. Belotelov, L. Bi, *ACS Photonics* **2022**, *9*, 1240.
[181] Q. Li, J. van de Groep, A. K. White, J. H. Song, S. A. Longwell, P. M. Fordyce, S. R. Quake, P. G. Kik, M. L. Brongersma, *Nat. Nanotechnol.* **2022**, *17*, 1097.
[182] S. Venkatesh, X. Lu, H. Saeidi, K. Sengupta, *Nat. Electron.* **2020**, *3*, 785.
[183] Y. L. Sun, X. G. Zhang, Q. Yu, W. X. Jiang, T. J. Cui, *Science Bull.* **2020**, *65*, 883.
[184] A. M. Shaltout, V. M. Shalaev, M. L. Brongersma, *Science* **2019**, *364*, 6441.
[185] O. Tsilipakos, A. C. Tasolamprou, A. Pitilakis, F. Liu, X. Wang, M. S. Mirmoosa, D. C. Tzarouchis, S. Abadal, H. Taghvaee, C. Liaskos, A. Tsioliaridou, J. Georgiou, A. Cabellos-Aparicio, E. Alarcón, S. Ioannidis, A. Pitsillides, I. F. Akyildiz, N. V. Kantartzis, E. N. Economou, C. M. Soukoulis, M. Kafesaki, S. Tretyakov, *Adv. Opt. Mater.* **2020**, *8*, 2000783.
[186] H. Zhou, S. Zhang, S. Wang, Y. Yao, Q. Cai, J. Lin, X. Zheng, Z. Wang, Z. Tao, Q. He, L. Zhou, *Adv. Photon.* **2023**, *5*, 026005.
[187] X. Zang, B. Yao, L. Chen, J. Xie, X. Guo, A. V. Balakin, A. P. Shkurinov, S. Zhuang, *Light: Adv. Manuf.* **2021**, *2*, 148.
[188] L. Zhang, X. Q. Chen, S. Liu, Q. Zhang, J. Zhao, J. Y. Dai, G. D. Bai, X. Wan, Q. Cheng, G. Castaldi, V. Galdi, T. J. Cui, *Nat. Commun.* **2018**, *9*, 4334.
[189] G. K. Shirmanesh, R. Sokhoyan, P. C. Wu, H. A. Atwater, *ACS Nano* **2020**, *14*, 6912.
[190] H. Chen, S. Nanz, A. Abass, J. Yan, T. Gao, D.-Y. Choi, Y. S. Kivshar, C. Rockstuhl, D. N. Neshev, *ACS Photonics* **2017**, *4*, 3031.
[191] H. Yang, H. Liu, B. Song, Y. Li, D. Meng, B. Chen, P. Hu, Y. Wang, T.-H. Ou, M. L. Povinelli, W. Wu, *Nanophotonics* **2020**, *9*, 1401.
[192] D. C. Zografopoulos, O. Tsilipakos, *Mater. Adv.* **2023**, *4*, 11.
[193] D. Hao, Y. Zhang, D. Yang, R. Li, D. Zhao, Z. Zhang, S. Wang, W. Jin, H. Tian, J. Duan, F. Fan, S. Chang, R. Maro, L. Ma, *Opt. Lett.* **2022**, *47*, 6101.
[194] L. Huang, R. Jin, C. Zhou, G. Li, L. Xu, A. Overvig, F. Deng, X. Chen, W. Lu, A. Alu, A. E. Miroshnichenko, *Nat. Commun.* **2023**, *14*, 3433.

Danni Hao obtained her Ph.D. degree in electronics and electrical engineering in 2018 from University of Glasgow. Then, she joined Tianjin International Center for Nanoparticles and Nanosystems, Tianjin University and worked as a postdoctoral researcher under the supervision of Prof. Lei Ma. Her research interests include plasmonic devices, metamaterial and metasurface based biosensing technology, and terahertz wave modulation.

Jinwei Liu received his M.S. degree from Tianjin University of Technology in 2023. Currently, he is a Ph.D. candidate at Tianjin International Center for Nanoparticles and Nanosystems in Tianjin University. His main research interests include electromagnetic metamaterials and terahertz sensors.

Pinggen Zou received his Bachelor of Engineering degree in Hebei University of Technology in 2021. He is currently pursuing a Master's degree in Optical Engineering at Tianjin International Center for Nanoparticles and Nanosystems in Tianjin University. His research encompasses terahertz metamaterials, quasiperiodic structures, data mining, machine learning, and optimization.

Yi Zhang received his M.S. degree from Tianjin International Center for Nanoparticles and Nanosystems, Tianjin University in 2023. His main research interests include THz tunable metamaterials and flexible metamaterials.

Ramiro Moro received his Ph.D. degree from Georgia Institute of Technology in 2003. After three years postdoc training at the University of South California, he took a tenure-track assistant professor position in University of Camon and tenured to an associated professor in 2012. Since 2020, he moved to Tianjin International Center for Nanoparticles and Nanosystems as a full professor until 2023. His main research focuses on cluster physics.

Lei Ma (Corresponding author) earned his Ph.D. degree from Nanjing University in 2010. Then he had his Postdoc training in Brown University and Georgia Tech. From 2016, he took a full professor position in Tianjin University. His research mainly focuses on graphene electronics related physics and cluster physics as well as the instrumentation of mass spectrometer and high resolution photoelectrometer.